Recent methods for numerical simulation of turbulent combustion in gas turbines

L. Selle*, G. Lartigue*, L. Benoit* and T. Poinsot **
*CERFACS, CFD team, 31057 Toulouse Cedex
** IMF Toulouse, 31400 Toulouse CEDEX, France

December 22, 2003

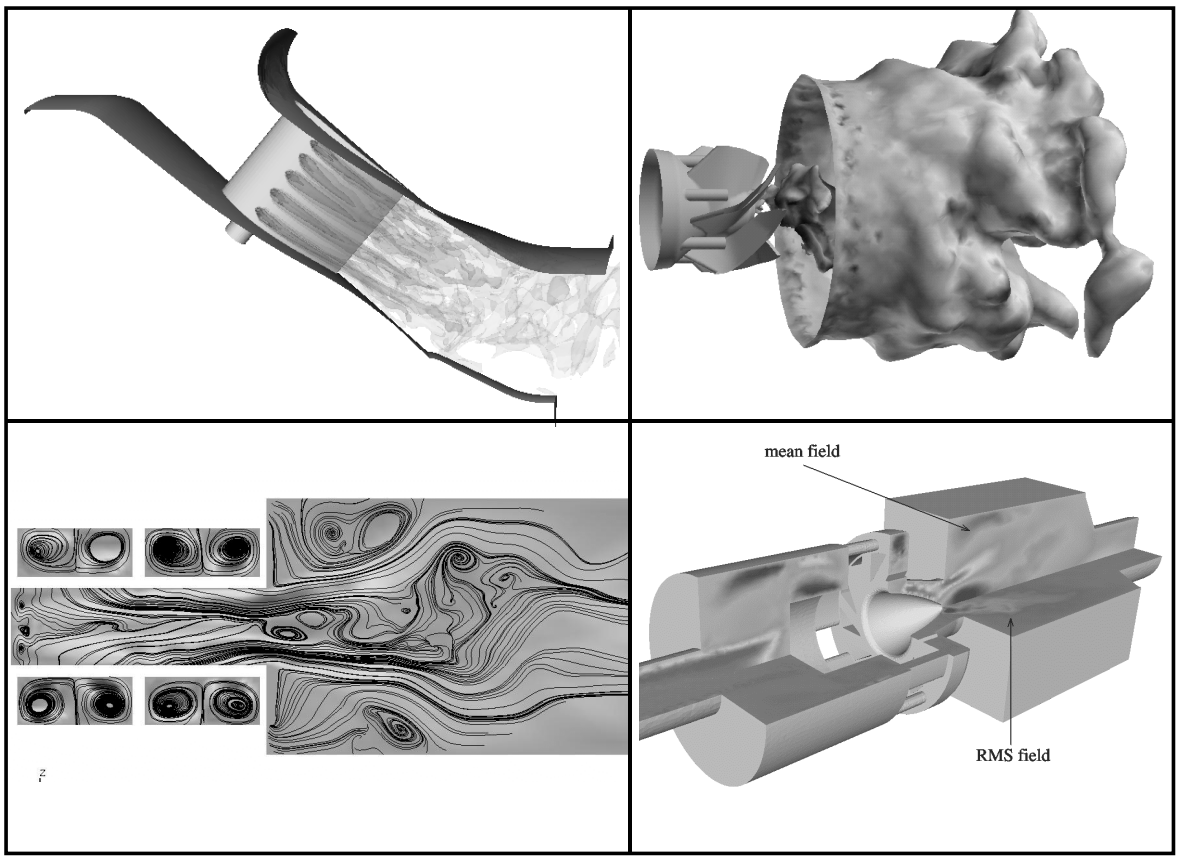

Abstract

Numerical simulations for gas turbines rely mostly on Reynolds Averaged Navier Stokes simulations (RANS) but also on more recent techniques such as Large Eddy Simulations which provide insights into unsteady combustion phenomena such as ignition, flashback, quenching or combustion instabilities. RANS techniques for combustion constitute now classical tools in the CFD community and will not be described here. These tools have also reached certain limits in gas turbines flows. In such configurations, strongly swirling flows constitute difficult cases for RANS: the existence of very strong hydrodynamic unstable modes such as Precessing Vortex Cores (PVC) requires intrinsically unsteady approaches. Moreover, acoustics and coupled acoustics / combustion flows are important in gas turbines and can change the nature of the flow drastically. For these interactions, RANS is not adequate and must be replaced by LES and by acoustic codes which can predict the acoustic field in the turbine.

This paper describes recent tools developed for LES in gas turbines and shows examples of applications in two configurations:

- a large scale burner (typical of high power industrial gas turbine) installed on a square combustion chamber in Karlsruhe and
- a prototype of small aeronautic gas turbine burner developed within the European Preccinsta project.

Both non-reacting and reacting flow cases are discussed. LES results are compared to experimental data in terms of axial and azimuthal velocities (mean and RMS), averaged temperature and existence of natural instabilities such as PVC (precessing vortex core). For these complex geometries, results demonstrate the capacity of the LES to predict the mean flow, with and without combustion as well as its main unstable modes: it is shown for example that the PVC mode is very strong for the cold flow but is damped with combustion in both configurations. This paper also shows the necessity of complementing LES results with acoustic analysis to understand and predict the various combustion modes observed in a combustor.

Contents

Chapter 1

Introduction

The design of modern combustion chambers for gas turbines rely heavily on numerical simulations. The most widely used tool for such simulations is RANS (Reynolds Averaged Navier Stokes) which predicts the mean values of all parameters in the chamber (velocity field, temperature, density and mass fractions). Even though these mean fields are essential ingredients of a successful design process, recent research has shown that they had to complemented by other CFD tools. These tools focus on the prediction of unsteady fields and on the coupling between the reacting flow and the acoustic field.

The motivation to develop such tools comes from the difficulties encountered in real devices: when gas turbines burners and chambers are improved, unexpected problems keep appearing in many cases. These problems include flame flashback, quenching, combustion oscillations. All these phenomena cannot be studied without specific unsteady tools. The objective of this paper is to describe two such tools:

- Large Eddy Simulation
- Acoustic codes

Large Eddy Simulations (LES) are powerful tools to study the dynamics of turbulent flames (see special issue of *Flow Turbulence and Combustion* (65, 2000) on LES of reacting flows or recent books on turbulent combustion: Peters 2000, Poinsot and Veynante 2001). Multiple recent papers have demonstrated the power of these methods (Angelberger et al. 2000, Caraeni et al. 2000, Colin and Rudgyard 2000 Desjardins and Frankel 1999, Pierce and Moin 1998, Pitsch and Duchamp de la Geneste 2002). For example, LES appears as one of the key tools to predict and study combustion instabilities encountered in gas turbines.

An important limitation of LES is its cost: the intrinsic nature of LES (full three-dimensional resolution of the unsteady Navier Stokes equations) makes it very expensive, even on today's computers so that faster tools are needed. Acoustic codes belong to this second category. These codes try to predict the global stability of a given combustion device by analyzing the amplification (or damping) of acoustic waves propagating through the entire combustion device. The most common versions of such codes describe acoustic propagation as one-dimensional waves and can describe combustion only through very simplified linear formulations such as the n-tau model (Crocco 1969, Kaufmann et al. 2002, Poinsot and Veynante 2001) or matrix formulations (Hsiao et al. 1998, Krueger et al. 2000, Paschereit et al. 2001, Polifke et al. 2001). In these formulations, the flame zone is viewed and modeled as a black box characterized only by its transfer function (or its matrix for matrix approaches) which essentially relates perturbations

of heat release in the flame to perturbations of inlet velocity. Acoustic codes are usually simple and fast.

Interestingly, LES and acoustic codes are linked in many recent approaches for gas turbines: LES is used to provide the mean fields, the unsteady fields and the flame transfer function. This flame transfer function can then be fed into the acoustic codes to predict the overall stability of the combustion chamber when it is connected to upstream and downstream ducts.

This paper describes recent progress in the field of LES, the basis of acoustic codes and examples of joint applications to two combustion chambers: a laboratory burner provided by Siemens and installed at University of Karlsruhe and another burner developed within the European project PRECCINSTA and equipped with a Turbomeca injection device. For both burners, cold and reacting flow results will be presented and the analysis of the results will be based on LES and acoustic data. Results show that:

- Cold flow results are dominated by the existence of a strong Precessing Vortex Core instability.
- The comparison between LDV and LES results shows that LES is extremely efficient to predict these swirling flows, not only for mean values but also for RMS values.
- For the two burners, this PVC is damped with combustion.
- The cold flow does not exhibit clear organized acoustic modes but the reacting flow does: these acoustic modes are a turning mode for the first burner and a quarter wave mode for the second. The acoustic codes confirm the results provided by the compressible LES data.

Generally speaking, these results confirm the potential of LES to analyze combustion instabilities but also demonstrate the necessity of coupling LES with simple tools to study acoustic phenomena in combustion chamber.

Chapter 2

Large Eddy Simulations for gas turbines

2.1 The specificities of LES for gas turbines

Most academic LES are often limited to fairly simple geometries for obvious reasons of cost and complexity reduction. In many cases, experiments are designed using simple shapes (two-dimensional (Angelberger et al. 2000, Duchamp de Lageneste and Pitsch 2001, Légier et al. 2000) or axisymmetrical configurations (Kempf et al. 2000, Pitsch and Steiner 2000) and simple regimes (low speed flows, fully premixed or fully non-premixed flames) to allow research to focus on the physics of the LES (subgrid scale models, flame / turbulence interaction model) and more generally to demonstrate the validity of the LES concept in academic cases. This approach is clearly adequate in terms of model development but it can also be misleading in various aspects when it comes to deal with complex flames in complex geometries, especially in real gas turbines for which specific problems arise:

- Real gas turbine geometries can not be meshed easily or rapidly with structured or block-structured meshes: up to now, most LES of reacting flows have been performed in combustion chambers where structured meshes were sufficient to describe the geometry. This is no longer the case in gas turbines and this brings additional difficulties. Indeed, on structured meshes, building high-order spatial schemes (typically 4^{th} to 6^{th} order in space) is easy and provides very precise numerical methods (Lele 1992,Ducros et al. 1996,Gamet et al. 1999). For complex geometries such structured meshes must be replaced by unstructured grids on which constructing high-order schemes is a more difficult task.

- Unstructured meshes also raise a variety of new problems in terms of subgrid scale filtering: defining filter sizes on a highly anisotropic irregular grid is another open research issue (Sagaut 2000, Scotti et al. 1997, Scotti et al. 1993, Vasilyev et al. 1998). Many LES models, developed and tuned on regular hexahedral grids, perform poorly on the low-quality unstructured grids required to mesh real combustion chambers.

- LES validations are often performed in laboratory low-speed unconfined flames in which acoustics do not play a role and the Mach number remains small so that acoustics and compressibility effects can be omitted from the equations ("low-Mach number approximation": Pierce and Moin 1998,Kempf et al. 2000). In most real flames (for example in gas turbines), the Mach number can reach much higher values and acoustics are important so that taking into account compressibility effects becomes mandatory. This leads to a significantly heavier computational task: since, acoustic waves propagate faster than

the flow, the time step becomes smaller and the boundary conditions must handle acoustic wave reflections (Poinsot and Veynante 2001). Being able to preserve computational speed on a large number of processors then also becomes an issue simply to obtain a result in a finite time.

- At the present time, it is impossible to perform a true LES everywhere in the flow and it will remain so for a long time. For example, the flow between vanes in swirled burners, inside the ducts feeding dilution jets or through multiperforated plates would require too many grid points. Compromises must be sought to offer (at least) robustness in places where the grid is not sufficient to resolve the unsteady flow.

These examples suggest that, for flames in gas turbines, work must concentrate on unstructured solvers, compressible flows, boundary conditions, robustness in poorly meshed zones, parallel efficiency. Many modeling aspects which were critical in simple laboratory flames (subgrid scale LES model for momentum, kinetic energy conservation, accuracy of chemistry description, etc) must now be combined with other (and sometimes more) critical problems: efficient unstructured solvers, subgrid scale LES models on "dirty" grids, boundary conditions adapted to acoustics...

Choosing a chemical scheme is another difficulty. For most laboratory flames, describing chemistry with only one variable is sufficient for LES (Williams 1985,Peters 2000,Poinsot and Veynante 2001): the progress variable is enough to compute fully premixed flames and the mixture fraction is adequate for perfectly non-premixed piloted flames such as the Sandia flames (Combustion Research Facility division at Sandia: http://www.ca.sandia.gov/crf/index.html). In real gas turbines, however, the combustion regime is much more complex and more "robust" models are required to handle flames which are typically partially premixed with a full range of local equivalence ratios and mixing levels.

2.2 An example of LES solver

To illustrate the structure of a LES code, the solver AVBP (see www.cerfacs.fr/cfd/ CFD-Web.html) is described here, starting with the numerical method, the flame / turbulence subgrid model and the reduced chemical scheme for methane / air combustion.

2.2.1 Numerical method for compressible reacting LES

The full compressible Navier Stokes equations are solved on hybrid (structured and unstructured) grids. Subgrid stresses are described by the WALE model (Nicoud and Ducros 1999). The flame / turbulence interaction is modeled by the Thickened Flame (TF) model (Angelberger et al. 2000, Colin et al. 2000). The numerical scheme is explicit in time: various tests performed with implicit schemes have shown that the gain was not significant. The main caution to perform correctly with explicit schemes for LES is to ensure that the mesh is as regular as possible and avoid very small mesh size. The scheme also provides third-order spatial accuracy and third-order time accuracy (Colin et al. 2000). Tests performed during this study have demonstrated that the third-order spatial accuracy of the solver is necessary to obtain precise LES results on unstructured meshes for the reacting cases. It is less critical for cold flow.

AVBP also handles variable heat capacities: species enthalpies are tabulated and the mean heat capacity is determined as a function of temperature and species mass fractions Y_k. Therefore, local quantities such as the mean molecular weight W or the ratio of heat capacities γ are not constant. This introduces significant additional complexities in the numerical method, especially near boundaries where classical characteristic methods such as NSCBC (Poinsot and Lele 1992) must be replaced by a more complex technique (Baum et al. 1994, Lartigue et al. 2003). In the two burners studied here, the walls of the combustion chambers are treated as adiabatic walls. Both no-slip and law-of-the-wall formulations have been used on walls with very limited differences on the results.

The code is fully parallel: this condition is necessary to produce the CPU power required for LES. Typical runs are performed on grids of 2.5 millions elements on 64 processors. For such runs, the speed up is close to 60.

2.2.2 A model for flame/turbulence interaction: the Thickened Flame

The two burners presented here are burning in only fully premixed modes. Multiple studies have concentrated on LES of diffusion flames (Forkel and Janicka 2000, Pierce and Moin 1998, Pitsch and Steiner 2000) while premixed cases have received less attention (Chakravarthy and Menon 2000, Fureby and Möller 1995, Pitsch and Duchamp de la Geneste 2002, Weller et al. 1998). Indeed, infinitely fast chemistry assumptions constitute a useful path for LES of diffusion flames. Such assumptions cannot be used for premixed flames, however: modelling the interaction between flame and turbulence in premixed combustion systems requires to track the flame front position, leading to a problem which is more difficult to handle than most diffusion flames. The natural technique to track the flame would be to solve its inner structure but this is impossible on typical LES meshes because premixed flame fronts are too thin. Two methods can then be used to propagate turbulent flame fronts on LES meshes:

- bring the flame thickness to zero and propagate the flame front as a thin interface: this is the principle of the G-equation method (Peters 2000, Pitsch and Duchamp de la Geneste 2002),
- thicken the flame so that it can be resolved on the LES mesh while still propagating at the same speed as the unthickened flame: this is the principle of the TF (Thickened Flame) model (Colin et al. 2000, Poinsot and Veynante 2001).

In the present work, the standard TF model developed by Colin *et al.* (Colin et al. 2000) is used: in this model, preexponential constants and transport coefficients are both modified to offer thicker reaction zones that can be resolved on LES meshes. The fundamental property justifying this approach has been put forward by Butler and O'Rourke (Butler and O'Rourke 1977) by considering the balance equation for the k-species mass fraction Y_k in a one-dimensional flame of thermal thickness δ_L^0 and speed s_L^0:

$$\frac{\partial \rho Y_k}{\partial t} + \frac{\partial \rho u Y_k}{\partial x} = \frac{\partial}{\partial x}\left(\rho D_k \frac{\partial Y_k}{\partial x}\right) + \dot{\omega}_k\left(Y_j, T\right) \tag{2.1}$$

Modifying this equation to have:

$$\frac{\partial \rho Y_k^{th}}{\partial t} + \frac{\partial \rho u Y_k^{th}}{\partial x} = \frac{\partial}{\partial x}\left(\rho F D_k \frac{\partial Y_k^{th}}{\partial x}\right) + \frac{1}{F}\dot{\omega}_k\left(Y_j^{th}, T^{th}\right) \tag{2.2}$$

leads to a "thickened" flame equation where F is the thickening factor and exponent th stands for thickened quantities. Introducing the variable changes $X = x/F$; $\Theta = t/F$ leads to:

$$\frac{\partial \rho Y_k^{th}}{\partial \Theta} + \frac{\partial \rho u Y_k^{th}}{\partial X} = \frac{\partial}{\partial X}\left(\rho D_k \frac{\partial Y_k^{th}}{\partial X}\right) + \dot{\omega}_k\left(Y_j^{th}, T^{th}\right) \tag{2.3}$$

which has the same solution as Eq. (2.1) and propagates the flame front at the same speed s_L^0. However, $Y_k^{th}(x,t) = Y_k(x/F, t/F)$ showing that the flame is thickened by a factor F. The thickened flame thickness is $\delta_L^1 = F\delta_L^0$. Choosing sufficiently large values of F allows to obtain a thickened flame which can be resolved on the LES mesh. Typically, if n is the number of mesh points within the flame front (n is of the order of 5 to 10) and Δx the mesh size, the resolved flame thickness δ_L^1 is $n\Delta x$ so that F must be $F = n\Delta x/s_L^0$. Note that F is not an additional parameter of the model but is imposed by the previous relation as soon as the mesh is created. For the computation of most flames using TF model, values of F ranging from 5 to 50 are sufficient to resolve the flame front on meshes corresponding to present computer capabilities. In the framework of LES, this approach has multiple advantages: when the flame is a laminar premixed front, the TF model propagates it at the laminar flame speed exactly like in a G equation approach. However, this flame propagation is due to the combination of diffusive and reactive terms which can also act independently so that quenching (near walls for example) or ignition may be simulated. Fully compressible equations may also be used as required to study combustion instabilities.

The thickening modification of the flame front also leads to a modified interaction between the turbulent flow and the flame: subgrid scale wrinkling must be reintroduced. This effect can be studied and parametrized using an efficiency function E derived from DNS results (Angelberger et al. 1998, Charlette et al. 2002, Colin et al. 2000). This efficiency function measures the subgrid scale wrinkling as a function of the local subgrid turbulent velocity u'_{Δ_e} and the filter width Δ_e. In practice, the diffusion coefficient D_k is replaced by EFD_k and the preexponential constant A by AE/F so that the conservation equation for species k is:

$$\frac{\partial \rho Y_k^{th}}{\partial t} + \frac{\partial \rho u Y_k^{th}}{\partial x} = \frac{\partial}{\partial x}\left(\rho E F D_k \frac{\partial Y_k^{th}}{\partial x}\right) + \frac{E}{F}\dot{\omega}_k\left(Y_j^{th}, T^{th}\right) \tag{2.4}$$

Such an equation propagates the turbulent flame at a turbulent speed $s_T = Es_L^0$ while keeping a thickness $\delta_L^1 = F\delta_L^0$. In laminar regions, E goes to unity, and Eq. 2.4 simply propagates the front at the laminar flame speed s_L^0.

A central ingredient of the TF model is the subgrid scale wrinkling function E. For this work, the initial model of Colin *et al.* (Colin et al. 2000) was used to express E as a function of the local filter size Δ_e, the local subgrid scale turbulent velocity u'_{Δ_e}, the laminar flame speed s_L^0, the laminar and the flame thicknesses δ_L^0 and δ_L^1:

$$E = \frac{\Xi(\delta_L^0)}{\Xi(\delta_L^1)} = \frac{1 + \alpha\Gamma\left(\frac{\Delta_e}{\delta_L^0}, \frac{u'_{\Delta_e}}{s_L^0}\right)\frac{u'_{\Delta_e}}{s_L^0}}{1 + \alpha\Gamma\left(\frac{\Delta_e}{\delta_L^1}, \frac{u'_{\Delta_e}}{s_L^0}\right)\frac{u'_{\Delta_e}}{s_L^0}} \tag{2.5}$$

where the function Γ corresponds to the integration of the effective strain rate induced by all scales affected by the artificial thickening, i.e. between the Kolmogorov η_K and the filter Δ_e

scales. α is a model parameter which scales as $\alpha \propto Re^{-\frac{1}{2}}$ (Colin et al. 2000). Γ is written as:

$$\Gamma\left(\frac{\Delta_e}{\delta_L^1}, \frac{u'_{\Delta_e}}{s_L^0}\right) = 0.75 \exp\left[-\frac{1.2}{\left(u'_{\Delta_e}/s_L^0\right)^{0.3}}\right]\left(\frac{\Delta_e}{\delta_L^1}\right)^{\frac{2}{3}} \tag{2.6}$$

The subgrid scale turbulent velocity is evaluated as: $u'_{\Delta_e} = 2\Delta_x^3|\nabla^2(\nabla \times \overline{u})|$, where Δ_x is the grid size. This formulation provides an estimate of the subgrid scale velocity which is unaffected by dilatation (Colin et al. 2000). Note that the filter size Δ_e may differ from Δ_x. It was suggested by Colin (Colin et al. 2000) to choose $\Delta_e = 10\Delta_x$.

The LES studies of Angelberger *et al.* (Angelberger et al. 2000) and Colin *et al.* (Colin et al. 2000) as well as various other tests have shown that Eq. 2.5 was adequate to predict subgrid scale wrinkling. In this work, a thickening factor $F = 25$ was used. Eq. 2.5 was developed and tested with single-step chemical schemes. Since the present study uses a two-step mechanism, additional DNS were performed to study the TF approach combined with a two-step chemical scheme (Selle et al. 2002) and to check whether the existing efficiency functions proposed in (Angelberger et al. 1998, Colin et al. 2000) or (Charlette et al. 2002) could be used without modification. Results showed that the two chemical reaction rates follow exactly the same evolution during these flame vortex interactions. These DNS suggest that, for the investigated range of parameters, the premixed flame acts as a flamelet distorted by flow motions even for low values of the length scale ratio $r/(F\delta_l^0)$, where r is the length scale on the vortices interacting with the flame front. Moreover, the effective strain rates induced by the vortices on the flame front and extracted from these DNS are in close agreement with (Angelberger et al. 1998, Colin et al. 2000) findings. Accordingly, the efficiency functions derived in (Angelberger et al. 1998, Charlette et al. 2002, Colin et al. 2000) were used without any modifications with the present two-step chemical scheme.

2.2.3 Reduced chemical scheme for LES

Both burners studied here use methane / air flames. The chemical schemes used for these flames are described here. In a TF model the complexity of chemical schemes must remain limited because all species are explicitely resolved. Up to now, only simple one-step chemical schemes have been used in TF models (Angelberger et al. 2000, Colin et al. 2000). In the present study, a two-step scheme is introduced to capture CO and predict more adequate flame temperatures as an intermediate step towards more complex schemes (typically four-step schemes such as (Jones and Lindstedt 1988)).

The chemical scheme (called 2sCM2) takes into account six species (CH_4,O_2, CO_2, CO, H_2O and N_2) and two reactions:

$$CH_4 + \frac{3}{2}O_2 \quad \longrightarrow \quad CO + 2H_2O \tag{2.7}$$

$$CO + \frac{1}{2}O_2 \quad \longleftrightarrow \quad CO_2 \tag{2.8}$$

The first reaction (2.7) is irreversible whereas the second one (2.8) is reversible and leads to an equilibrium between CO and CO_2 in the burnt gases. The rates of reaction (2.7) and (2.8) are

A_1	$n_1^{CH_4}$	$n_1^{O_2}$	E_{a1}	A_2	n_2^{CO}	$n_2^{O_2}$	$n_2^{CO_2}$	E_{a2}
$2E15$	0.9	1.1	34500	$2E9$	1	0.5	1	12000

Table 2.1: Rate constants for the 2sCM2 scheme: the activation energies are in cal/moles and the preexponential constants in cgs units.

respectively given by:

$$q_1 = A_1 \left(\frac{\rho Y_{CH_4}}{W_{CH_4}}\right)^{n_1^{CH_4}} \left(\frac{\rho Y_{O_2}}{W_{O_2}}\right)^{n_1^{O_2}} \exp\left(-\frac{E_{a1}}{RT}\right) \tag{2.9}$$

$$q_2 = A_2 \left[\left(\frac{\rho Y_{CO}}{W_{CO}}\right)^{n_2^{CO}} \left(\frac{\rho Y_{O_2}}{W_{O_2}}\right)^{n_2^{O_2}} - \left(\frac{\rho Y_{CO_2}}{W_{CO_2}}\right)^{n_2^{CO_2}}\right] \exp\left(-\frac{E_{a2}}{RT}\right) \tag{2.10}$$

where the parameters are provided in Table 2.1.

Modelling transport by molecular diffusion also requires attention: laminar flame codes such as PREMIX use polynomial fits for diffusion coefficients D_k. This precise but expensive technique may be replaced by a simpler approximation based on the observation that the individual Schmidt numbers of species $S_c^k = \nu/D_k$ are almost constant in many air / hydrocarbon flames. Therefore, in AVBP, the diffusion coefficient D_k of species k is obtained as $D_k = \nu/S_c^k$ where ν is the viscosity and S_c^k the fixed Schmidt number of species k. The Schmidt number values used in the present simulations are given in Table 2.2. In most cases, these values correspond to the PREMIX values measured in the burnt gases. The Prandtl number is set to 0.68. With this parameter set, the agreement between flame profiles obtained using AVBP or PREMIX with the same chemical scheme is excellent (Fig. 2.1).

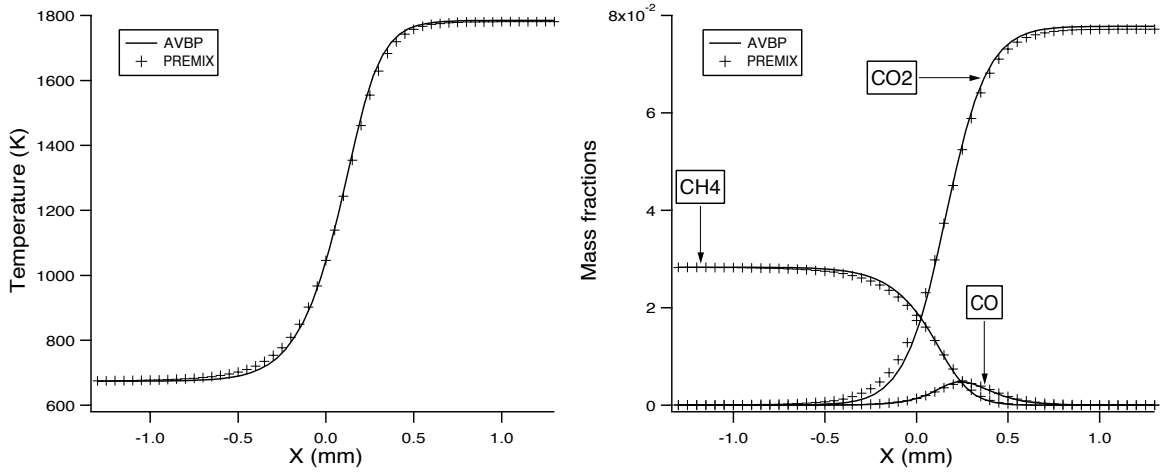

Figure 2.1: Comparison of AVBP and PREMIX for a laminar one-dimensional flame at $\phi = 0.5$. The fresh gas temperature is 673 K.

This scheme is directly implemented into the LES code. Its first advantage compared to a single-step scheme is to provide more accurate adiabatic flame temperatures. Fig. 2.2 compares the maximum flame temperatures obtained with AVBP and PREMIX using the full GRI mechanism. For 2sCM2, AVBP and PREMIX predict the same maximum flame temperature,

CH_4	CO_2	CO	O_2	H_2O	N_2
0.68	0.98	0.76	0.76	0.6	0.75

Table 2.2: Schmidt numbers.

confirming that the thermodynamical data of AVBP is correct. 2sCM2 overestimates the maximum flame temperaturecompared to GRImech by 100 K for rich cases but is very accurate for lean mixtures. The laminar flame speeds are also well predicted on the lean side (Fig. 2.3) but deviate from the exact results for rich cases. For the present cases, an equivalence ratio of 0.5 was used for configuration 1 and of 0.7 to 0.75 for configuration 2: for such lean cases, the AVBP predictions are very precise.

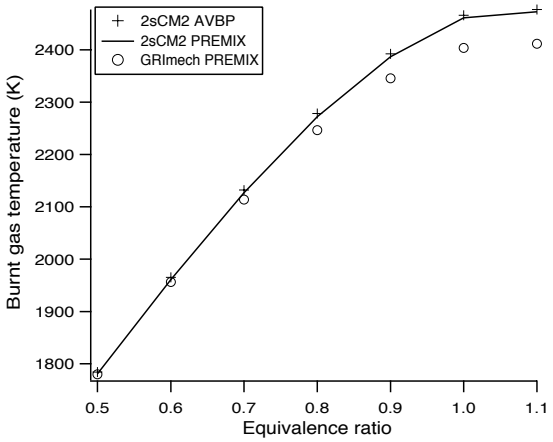

Figure 2.2: Burnt gas temperature (K).

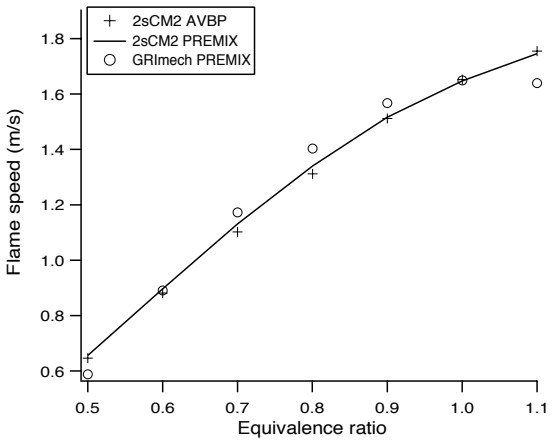

Figure 2.3: Laminar Flame speed s_L^0 $(m.s^{-1})$.

Chapter 3

Acoustic tools for gas turbines

The problem of the coupling between flames and acoustic fields is old and unsolved. The famous example of the singing flame of Lord Rayleigh (Rayleigh 1878 demonstrated that this coupling can be very strong: it is sufficient to place a flame in a duct to observe (for certain conditions) a very intense acoustic field at a discrete frequency. For these conditions, optical diagnostics or temperature measurements reveal a strong movement of the flame at the same frequency. Modeling such phenomena has been the target of multiple studies in the past (see for example Candel et al. 1996, Crighton et al. 1992, Poinsot and Veynante 2001, Williams 1985). In this paper, we will focus on two tools which are becoming almost 'standard' tools in most gas turbine companies and research centers. The first one (one-dimensional, described in Section 3.1) solves for longitudinal low-frequency waves in networks of ducts representing the compressor passages, the combustion chamber and the turbine. The second one (three-dimensional, described in Section 3.2) solves for all modes (longitudinal and transverse) in a combustion chamber. In both cases, the derivation of the model is too long to be fully detailed here and the reader is referred to (Poinsot and Veynante 2001) for a more complete description. The common approach in both models is to linearize the compressible reacting equations around a mean state and to solve for the eigenmodes of these linearized problems with adequate boundary conditions.

The intrinsic limitations of acoustic codes are significant but they remain essential tools for the following reasons:

- The linearization is valid only for small amplitude perturbations, a condition which is obviously not true when limit cycles typical of combustion instabilities are observed in gas turbines. Such limit cycles can be strong enough to induce flow reversal at the combustor inlet section (Keller et al. 1981): clearly, it is not possible then to view the velocity perturbation as a small variation around the mean state. However, this assumption is valid when the instability grows (Poinsot et al. 1988) and helps to determine the unstable modes: such modes have to appear and grow before they reach a limit cycle and any analysis able to study them during this early phase is of interest.

- Most acoustic tools work on linear regimes for which each oscillatory mode is independent of other modes. Now, many combustion instabilities exhibit non-linear coupling where high-frequency modes couple with low-frequency oscillations: classical papers from Rogers and Marble for example (Rogers and Marble 1956) mention such coupling. They were also observed in the experiment of Poinsot et al. 1987 in which a 530 Hz mode (often called rumble) was systematically accompanied by a high-frequency mode

(called screech) at 3750 Hz. The fact that combustion instabilities involve more than one mode of oscillation is one of the basis of theories by Culick for example (Yang and Culick 1986). The tools presented below treat each mode individually and cannot simulate such phenomena.

- The description of the coupling between acoustics and combustion in such models is extremely crude.

Despite these limitations, such tools are useful because they run fast, can be used for design and can also be coupled now with LES and become more precise.

3.1 One-dimensional tools

Many gas turbines exhibit low-frequency oscillations (frequency f less than 300 Hz typically) for which the acoustic wavelength Λ is of the order of c/f (where c is the sound speed) which corresponds to a few meters. Since these wavelengths are much longer than the typical transverse size of the burner, it is possible to assume that only longitudinal planar waves propagate through the entire gas turbine. Assuming one-dimensional waves diminishes the complexity of the problem considerably and allows a resolution of the linearized problem by a simple matrix method (Poinsot and Veynante 2001). The geometry of the entire device can be subdivided into small one-dimensional elements which are connected by jump conditions. The input parameters of such codes are the section and length of each tube element. The sound speed in each tube is also needed. The main ideas of Soundtube are summarized in Fig. 3.1.

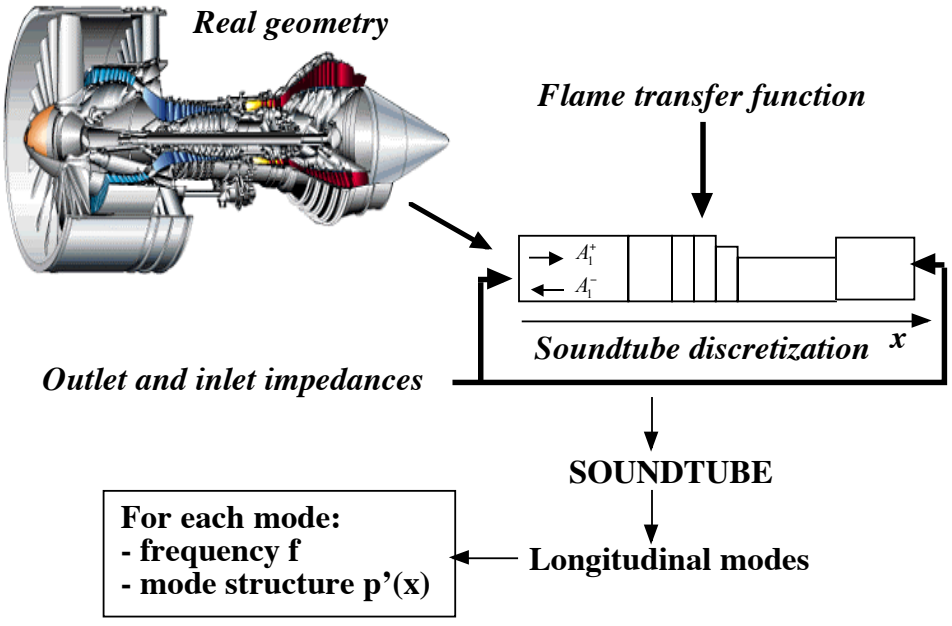

Figure 3.1: Principle of Soundtube, a one-dimensional acoustic network code for gas turbines

These tools are efficient but they have two weak points:

- Impedances at the inlet and the outlet of the domain are required and usually unknown. For example, if only the combustion chamber is solved for, the impedances of the compressor (upstream) and of the turbine (downstream) are needed: these impedances are difficult to obtain.

- In these modes the flame is viewed as a localized 'active' acoustic element (a source of unsteady volume flow) which is characterized by its transfer function betwen unsteady velocity and unsteady heat release (or volume source). This transfer function is generally unknown. It can be measured or computed using LES.

Such tools are one-dimensional but can be extended to networks with connections (called "one and a half" tools) to account for various one-dimensional ducts connected together. This is useful to describe the low-frequency modes found in gas turbines (associated to transverse of turning modes).

Note also that one-dimensional acoustic tools predict all longitudinal modes but also another acoustic mode which is quite famous in reacting systems: the so-called Helmholtz frequency (Kinsler et al. 1982) which is actually one of the longitudinal modes too. A Helmholtz resonator is created when a small duct is connected to a large plenum (certain combustion chambers actually match this description when they are terminated by a nozzle). Such a device is displayed in Fig. 3.2: this 'double-duct' arrangement consists of a cavity of volume V (height d and section S_o) fitted to a neck of area S and length L. This device acts like a spring (the pressure within the cavity) - mass (the gas within the neck) - resistance (the acoustic radiation on the opening) system and has a resonance frequency f_H given by:

$$f_H = \frac{c}{2\pi}\sqrt{\frac{S}{LV}} \tag{3.1}$$

where L is the neck length and c is the sound speed in the cavity.

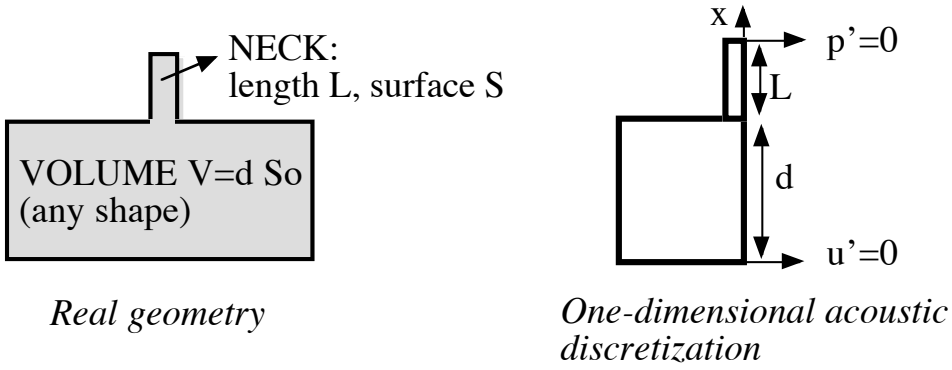

Figure 3.2: Helmholtz resonator (left) and 1D equivalent model (right): the 'double-duct'.

Viewed in a one-dimensional acoustic manner, the Helmholtz resonator is displayed on the right side of Fig. 3.2. For this configuration, Poinsot and Veynante 2001 provide a direct expression of the final equation which would be solved by a one-dimensional acoustic code (everything here is written in the absence of combustion but the conclusions would be the same with reaction):

$$cos(kd)cos(kL) - \Gamma sin(kd)sin(kL) = 0. \tag{3.2}$$

where Γ is the section ratio between volume V and neck: $\Gamma = S_o/S$. For low frequencies (as it is the case for the Helmholtz resonator), the wave number $k = 2\pi f/c$ is small and Eq. (3.2) becomes, to first order in k:

$$1 - \Gamma(kd)(kL) = 0. \quad \text{or} \quad f = \frac{c}{2\pi}\sqrt{\frac{S}{LV}} = \frac{c}{2\pi}\sqrt{\frac{1}{Ld\Gamma}} \tag{3.3}$$

which is exactly the classical expression (3.1) for a Helmholtz resonator. To confirm this analytic proof, Fig. 3.3 also displays the frequencies of the Helmholtz resonator and of the quarter wave mode given by Eq. (3.2) and computed with a one-dimensional acoustic tool as a function of the section ratio $\Gamma = S_o/S$. The geometry corresponds to Fig. 3.2. The values chosen for the application are: $c = 830$ m/s (corresponding to sound speed in burnt gases), $L = 0.06$ m and $d = 0.12$ m. For large values of Γ, both curves collapse.

A very interesting conclusion of Fig. 3.3 (illustrating a mistake which is often seen in the combustion community) is that the 'real' frequency of oscillation of the 'double duct' device displayed in Fig. 3.2 and computed either with Eq. (3.1) or with Eq. (3.2) can be significantly lower than the frequency f_Q of a constant section duct (dashed line in Fig. 3.3). For example, in a double duct device like Fig. 3.2, the total length of the device is $d + L$ and this frequency f_Q is usually evaluated by:

$$f_Q = c/(4(d+L)) \tag{3.4}$$

Therefore, considering the total length of a combustion chamber and evaluating the first quarter wave frequency f_Q using the total length of the chamber can be misleading: the first acoustic mode frequency can be much lower than f_Q. When the section ratio Γ goes to large values (in other words when the geometry exhibits strong localized section restrictions, like injectors), the acoustic frequency goes to zero like $1/\Gamma^{1/2}$ as shown by Eq. (3.3). As a result, predicting the first longitudinal mode frequency in a combustor can be a difficult exercice and it is recommended to use a one-dimensional acoustic solver (and not approximate quarter-wave formula like Eq. (3.4)).

3.2 Three-dimensional Helmholtz tools

Many combustors exhibit longitudinal oscillations but high-frequency transverse modes can be even more dangerous. In addition they are more difficult to study. Screech, for example, is a transverse mode observed in afterburners which can destroy an engine in a few seconds. The signature of high-frequency transverse modes is that the pressure field exhibits oscillations which have a structure along the flow axis but also along the normal to the flow axis. The tool presented in the previous section cannot be used anymore for such flows and more complete analysis are needed. These methods essentially extend the principle of the one-dimensional tool: start from the wave equation, linearize around the mean state and solve for its eigenmodes. In the general case, these eigenmodes are multidimensional. The general form of the Helmholtz equation in a reacting flow is (Poinsot and Veynante 2001,Crighton et al. 1992):

$$\nabla \cdot \left(c^2 \nabla p'\right) - \frac{\partial^2}{\partial t^2} p' = -(\gamma - 1)\frac{\partial \dot{\omega}_T}{\partial t} - \gamma p_0 \nabla \vec{u} : \nabla \vec{u} \tag{3.5}$$

where p' is the pressure perturbation, $\dot{\omega}_T$ is the unsteady local heat release and p_0 is the average pressure and c is the local sound speed. c changes considerably in a reacting flow: it depends

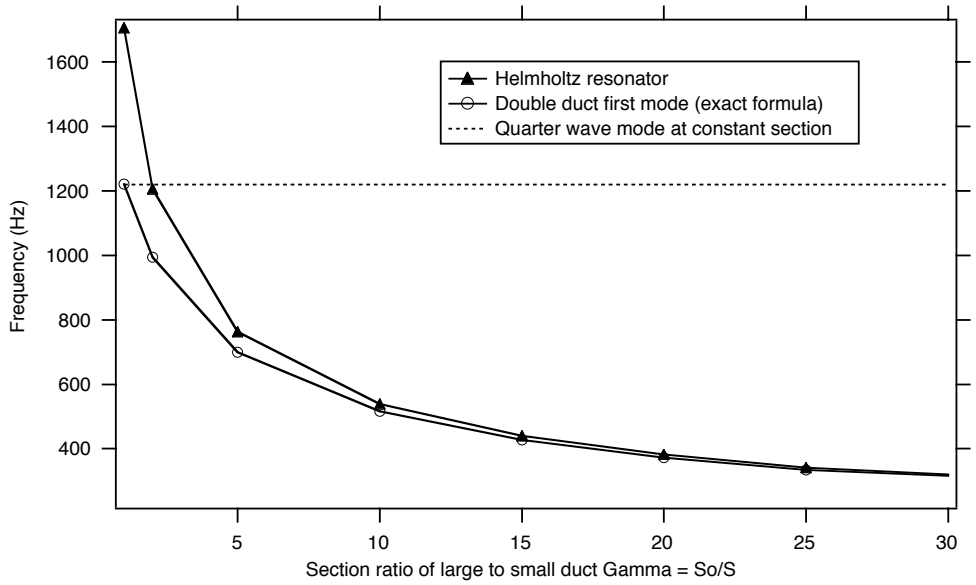

Figure 3.3: The frequencies of the Helmholtz resonator (Eq. (3.1)), the double-duct quarter-wave mode (Eq. (3.2)) of Fig. 3.2 and the quarter-wave mode assuming constant section as a function of the section ratio $\Gamma = S_o/S$ between the volume V and the neck.

on the local value of γ, on the mean molecular weight W and on temperature: $c = (\gamma RT/W)^{1/2}$ where $R = 8.32uSI$).

Table 3.1 compares the wave equation in non-reacting flows and in a reacting flow. For the non-reacting case, the $\nabla\vec{u} : \nabla\vec{u}$ term is retained: this term is responsible for turbulent flow noise. It is usually neglected in combustion applications because the second term (due to combustion) is larger. A complexity brought by combustion is the variable sound speed which must be kept in the ∇ operator and the additional source term found on the RHS terms for the pressure equation with combustion. This source term is responsible for combustion noise and instabilities. The linearized form of Eq. (3.5) is sufficient to capture the growth of unstable modes but non-linear extensions are required to describe non-linear effects seen in many limit-cycles.

Classical acoustics (c =constant)	$c^2\nabla^2 p' - \dfrac{\partial^2 p'}{\partial t^2} = -\gamma p_0 \nabla\vec{u} : \nabla\vec{u}$
Acoustics in reacting flows	$\nabla(c^2\nabla p') - \dfrac{\partial^2 p'}{\partial t^2} = -(\gamma-1)\dfrac{\partial \dot{\omega}_T}{\partial t} - \gamma p_0 \nabla\vec{u} : \nabla\vec{u}$

Table 3.1: Comparison of wave equations for non-reacting and reacting flows.

The wave equation is usually not solved in the time domain but in the frequency domain by assuming harmonic pressure variations at frequency $f = \omega/(2\pi)$ for pressure and for local heat release perturbations:

$$p' = P'(x,y,z)\exp(-i\omega t) \quad \text{and} \quad \dot{\omega}_T = \Omega'_T \exp(-i\omega t) \quad \text{with} \quad i^2 = -1 \tag{3.6}$$

Introducing Eq. (3.6) into Eq. (3.5) leads to the Helmholtz equation where the unknown quantity is the pressure oscillation amplitude P' at frequency f and the heat release perturbation field Ω'_T:

$$\nabla \cdot \left(c^2 \nabla P'\right) + \omega^2 P' = i\omega(\gamma - 1)\Omega'_T \tag{3.7}$$

This equation is the basis of three-dimensional Helmholtz codes. Knowing the sound speed (c) distribution, ie knowing the local composition and temperature, this equation provides the eigen frequencies ω_k and the associated structure of the mode $P'_k(x,y,z)$. At this point, two approaches of increasing complexity are found :

- First, the effects of the unsteady combustion can be neglected by setting $\Omega'_T = 0$. This is equivalent to finding the eigenmodes of the burner, taking into account the presence of the flame through the mean temperature field but neglecting the flame effect as an acoustic active element.
- In a second step, the active effect of combustion can be taken into account if a model linking Ω'_T and P' can be derived. This is usually the difficult part of the modeling: here again, LES is one of the only ways to obtain this information.

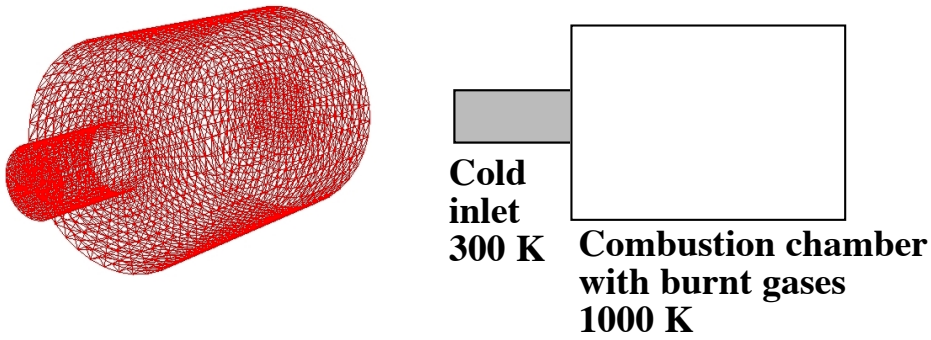

Figure 3.4: Example of application of AVSP: computation of the modes of a simple dump combustor.

The usual numerical techniques for Eq. (3.7) are based on finite element methods. In the present paper, only computations with inactive flames will be presented. Such computations are useful to identify complex mode shapes and evaluate their growth rate even in the absence of an active flame. The solver used for this study if AVSP developed by L. Benoit at CERFACS.

An example of application of AVSP is given in Fig. 3.4: a model combustor with a cold inlet and a homogeneous temperature combustion chamber is computed using AVSP. The length and diameter of the inlet pipe are 10 and 6 cm and the length and diameter of the combustion chamber are respectively 25 and 20 cm. All boundary conditions correspond to hard walls (imposed velocity). The results are displayed in Fig. 3.5.

The structures of two modes identified by AVSP are displayed in Fig. 3.5: the first mode (left figure) at 727 Hz is a longitudinal one (which would also be recovered by Soundtube). The second one (right figure) is a 1T-1L at 2211 Hz (first transverse - first longitudinal). For this second mode, the sides of the combustor near the dump plane act as pressure antinodes so that the axis of the combustion chamber is a velocity antinode. The existence of large velocity oscillations on the chamber axis could be an important source of oscillations in a real combustor and the example of Section 4 will present such an example.

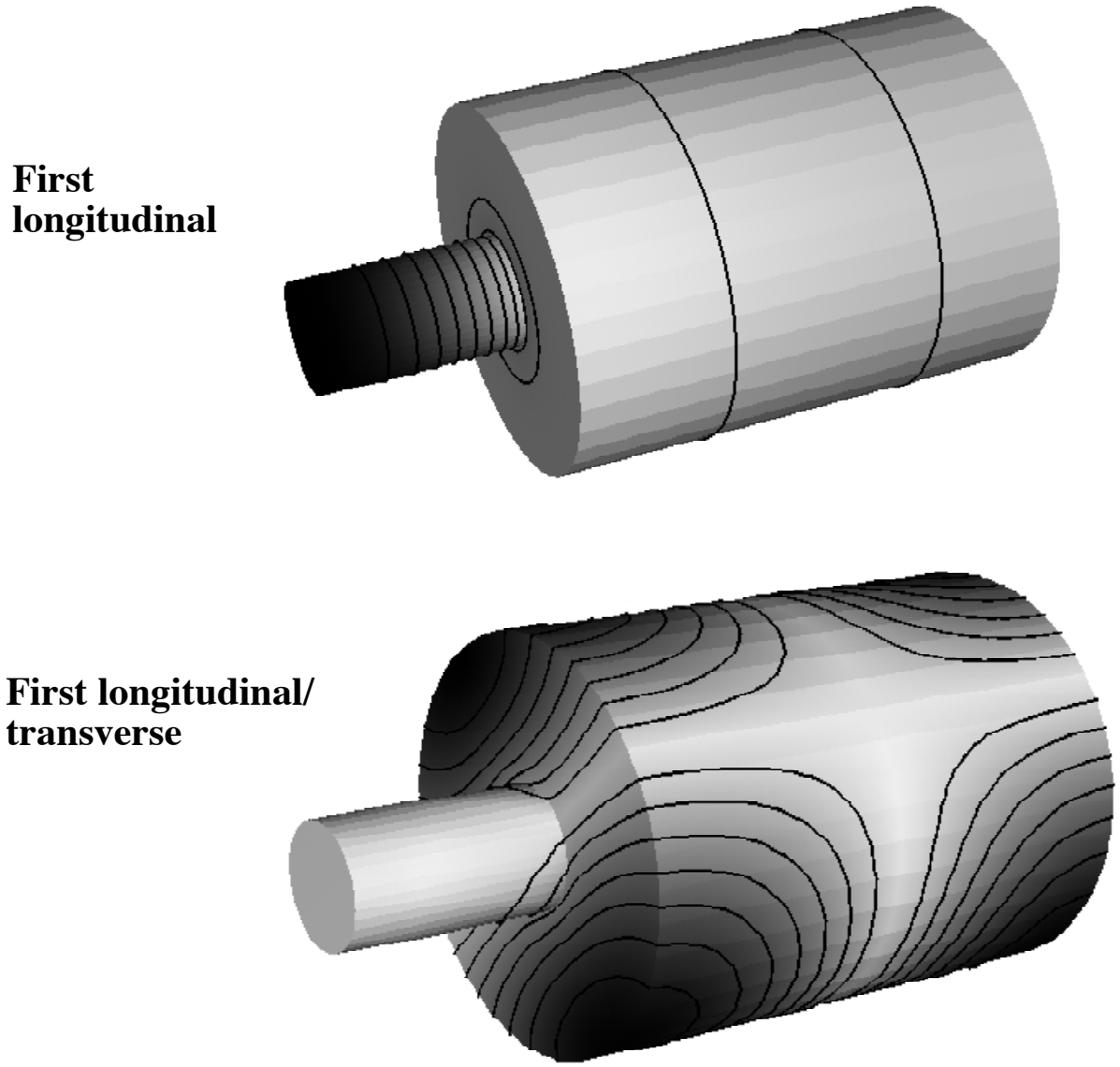

Figure 3.5: Results of AVSP for the burner of Fig. 3.4. The acoustic pressure amplitude P' is plotted on the walls of the chamber. Top: first longitudinal 1L mode (727 Hz). Bottom: first 1T-1L mode (2211 Hz).

Chapter 4

Application to configuration 1

4.1 Geometry and regime in configuration 1

The first example of application of the LES and acoustic tools is an industrial gas turbine burner (CAD data provided by Siemens PG). The grid contains 2381238 cells. Fig. 4.1 shows the main features of the burner: a central axial swirler (colored in dark) is used to inject and swirl air and, for certain regimes (not studied here), non premixed fuel. The main part of the combustion air as well as fuel (through holes located on both sides of the vanes used for swirling) is injected by the diagonal swirler. Its external surface is visualized in Fig. 4.1 by a wire type surface. For the present study, both axial and diagonal swirlers are fed with premixed air.

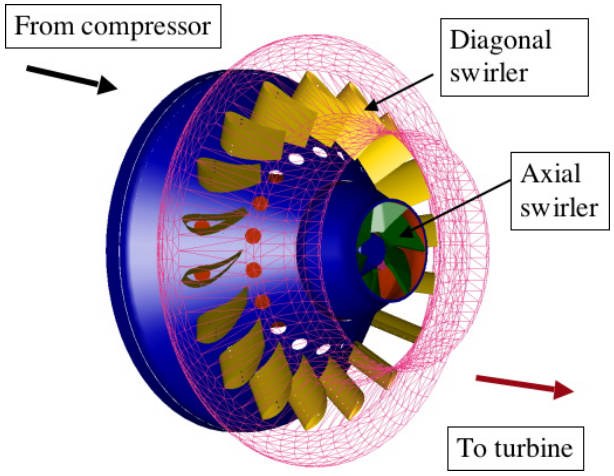

Figure 4.1: Burner: the vanes of the diagonal swirler are not computed.

In Karlsruhe University (ITS), this single SIEMENS burner (scale 1:1) is mounted on an atmospheric test rig. The combustion chamber has a square cross section with a truncated pyramid shape at the exit. Both the casing and the chamber walls allow optical access for velocity measurements by LDA. The burner is fired with natural gas (assumed to be mostly methane), and the air is pre-heated to 673K. The thermal power varies between 420kW (at $\Phi = 0.5$) and 810kW (at $\Phi = 0.83$). Measurements were performed at ITS Karlsruhe to characterize:

- the cold flow velocity field in terms of mean and RMS velocities using LDA techniques,

- the hot flow velocity field in terms of mean and RMS components as well as the mean temperature field using thermocouple data (The time response of the thermocouple was not sufficient to provide RMS temperature data).

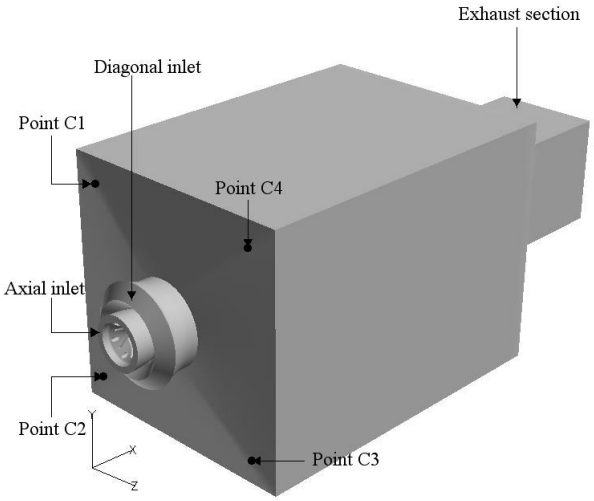

Figure 4.2: Burner mounted on ITS combustion chamber.

Measurements are performed in transverse cuts and at the outlet of the diagonal swirler as represented in Fig. 4.3. For the cold flow, there are 15 cuts ranging from $x/R = 0.37$ to $x/R = 4.17$, where R is the radius of the burner outlet. For the case with combustion, there are 6 cuts ranging from $x/R = 0.7$ to $x/R = 4.32$.

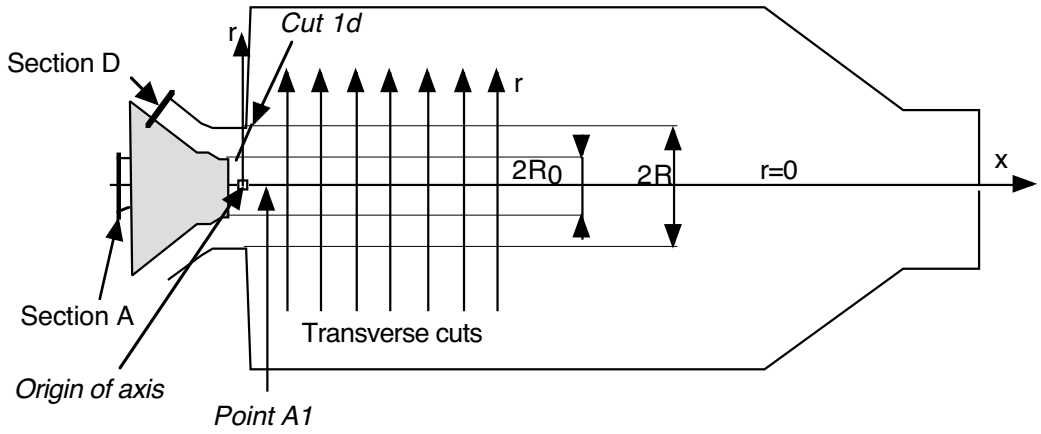

Figure 4.3: Burner mounted on ITS combustion chamber: location of LDV measurements.

4.2 Inlet conditions in configuration 1

Specifying boundary conditions is a difficult exercice in most LES. For configuration 1, the conditions to specify raise different difficulties for the axial and the diagonal swirlers.

The computation of the *axial swirler* begins upstream of the vanes: the flow in Section A (Fig. 4.3) is introduced along the x axis only without swirl. This clean condition avoids uncertainties in the specification of the boundary conditions. Of course, it is costly because the vanes of the axail swirler must be fully meshed and computed.

For the *diagonal swirler*, the problem is more difficult since computing completely this part of the burner would require a full computation of all vanes placed in the passage. At the moment, this is impossible and inlet conditions are specified just downstream of these vanes in Section D in Fig. 4.3. Velocities could not be measured in Section D; the LES however starts there and the inlet velocity profiles in this section are adjusted to match the first measurement section (Cut 1d in Fig. 4.3) in the burner under non-reacting cases.

Velocity measurements have been performed in various sections displayed on Fig. 4.3. The swirling velocity W and the velocity U_{22} normal to a plane parallel to the diagonal swirler exit plane (at an angle of 22 degrees compared to the vertical axis) are measured in the test section located close to the burner nozzle (cut 1d). Distances and velocities are respectively scaled by the burner radius R and the bulk velocity U_{bulk} defined by $U_{bulk} = \dot{V}/\pi R^2$ where $\dot{V}$ is the total volume flow rate through the burner.

Average profiles of axial and radial velocities at the exit of the diagonal burner are displayed in Fig. 4.4 and 4.5 (cut 1d in Fig. 4.3). In figures, symbols ($\circ$) denote experimental data while LES results are plotted with solid lines (———). No fluctuating velocity components are added to the inlet conditions: this incoming turbulence can be neglected compared to the turbulent activity in the chamber which is mainly due to the very high velocity gradients created by the swirling motion in the dump plane of the chamber.

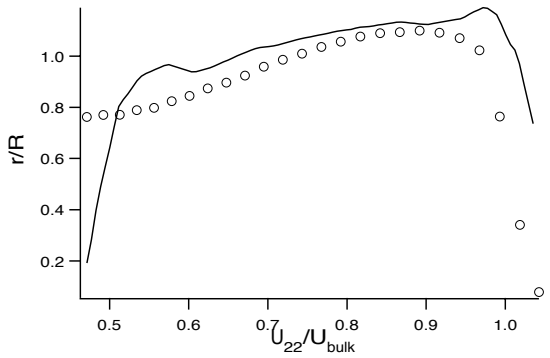

Figure 4.4: Normalized velocity U_{22}/U_{bulk} at the exit of the diagonal swirler (Cut 1d).

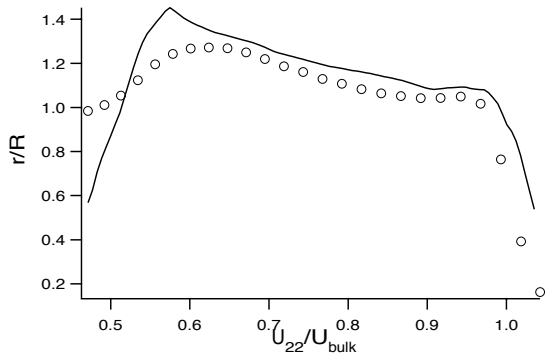

Figure 4.5: Normalized swirl velocity W/U_{bulk} at the exit of the diagonal swirler (Cut 1d).

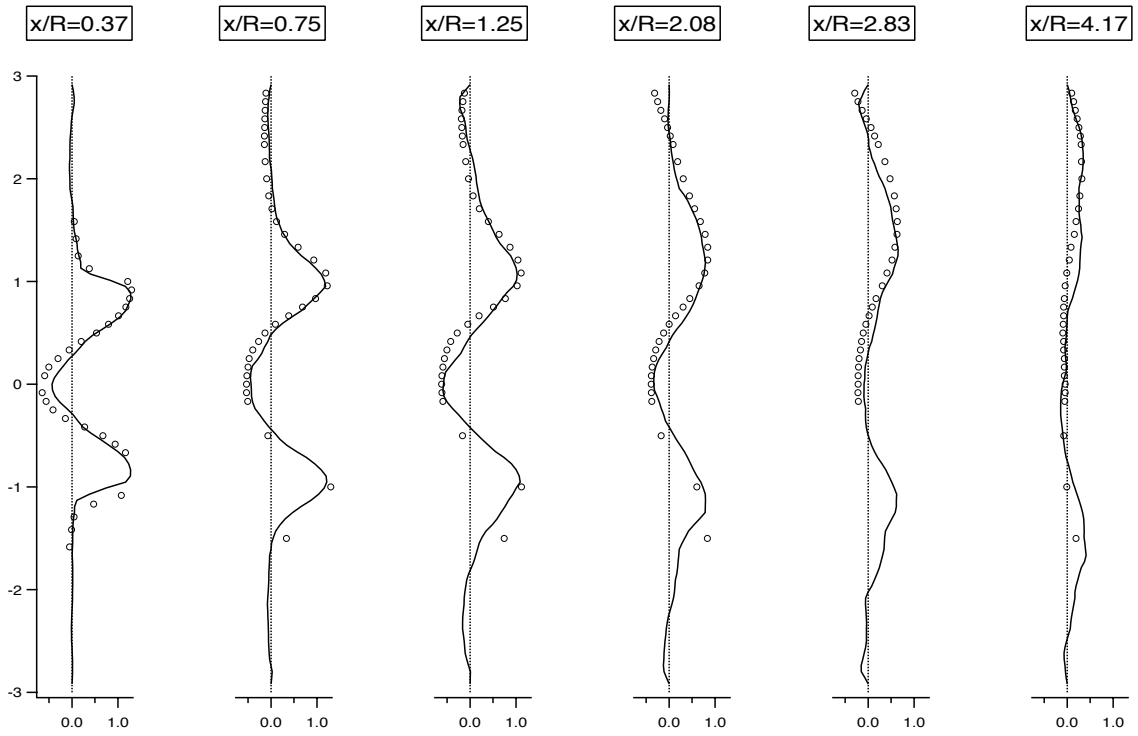

Figure 4.6: Cold flow mean axial velocity (U/U_{bulk}): ○ LDV; —— LES.

4.3 Non reacting flow in configuration 1

4.3.1 Averaged fields

In this section, LDV measurements (○) are compared to averaged LES results (——) at different downstream locations x in the combustor (Fig. 4.6 to 4.9). In Fig. 4.6 (axial velocity profiles) and 4.7 (swirling velocities), LES data are averaged over about 36 ms corresponding to two flow times through the entire combustion chamber at the bulk velocity. Only 6 downstream locations are displayed for clarity but 15 were investigated.

LES and experimental data predict the size, shape and intensity of the recirculation zone in very similar ways as well as the overall spreading of the turbulent swirling jet. Results are displayed for the whole size of the combustion chamber and not only for one half chamber to evidence symmetry defaults. Since the chamber is square and the injection device axisymmetric, average velocities are expected to be symmetrical versus the x-axis. However both experimental data and LES results are not perfectly symmetrical, especially downstream. This finding (which is quite usual in these flows) may indicate a lack of sampling of LES data but may also be due to an intrinsic difficulty in such flows to follow the symmetry of the geometry.

To plot the RMS profiles (Fig. 4.8 and 4.9), only the resolved part of the fluctuations is taken into account here and the agreement is good. This demonstrates that for this flow, most of the unsteady motion lies in large structures which are very well predicted by LES methods. Cut $x/R = 0.37$ in Fig. 4.9 shows that the largest fluctuations of the swirling component are located on the axis, and reach up to 60% of the bulk velocity. This will be explained in the following

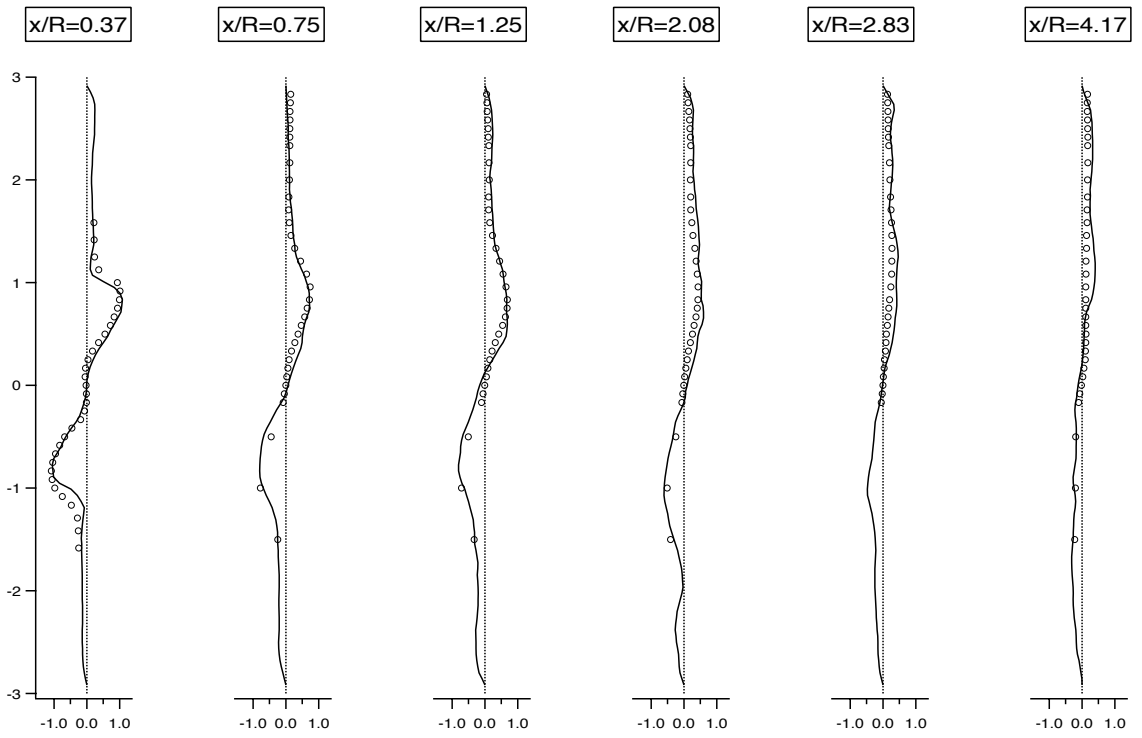

Figure 4.7: Cold flow mean swirling velocity (W/U_{bulk}): ○ LDV; —— LES.

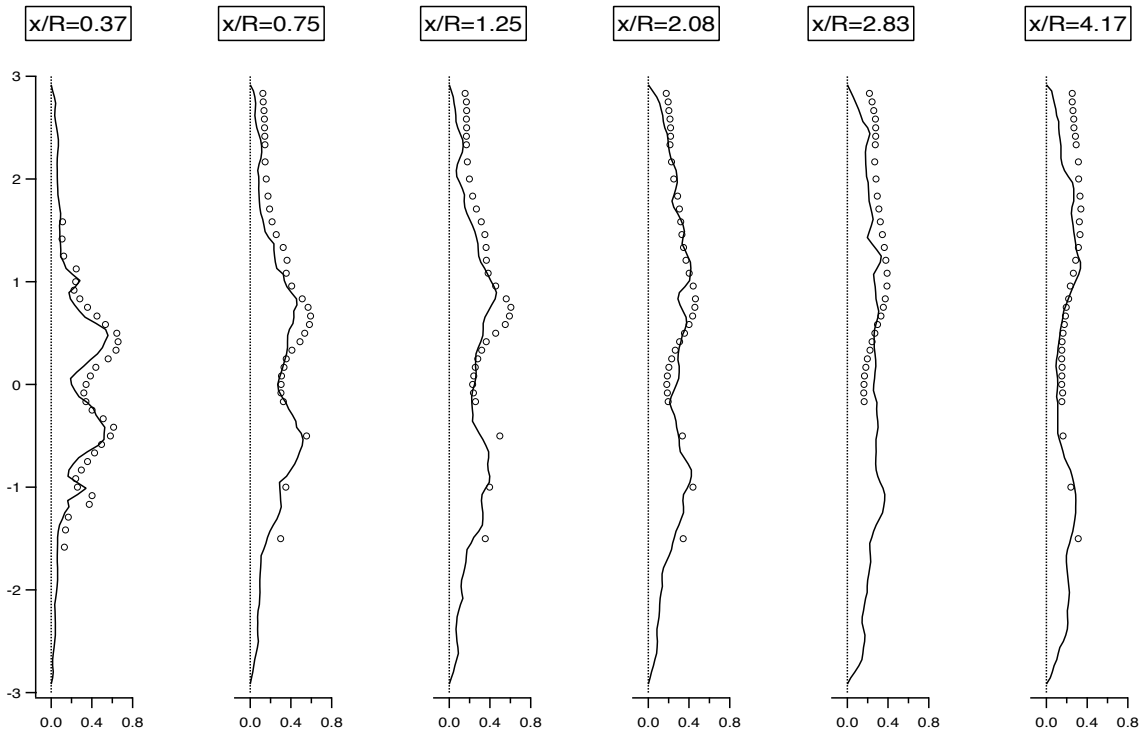

Figure 4.8: Cold flow axial velocity fluctuations (U'/U_{bulk}). ○ LDV; —— LES.

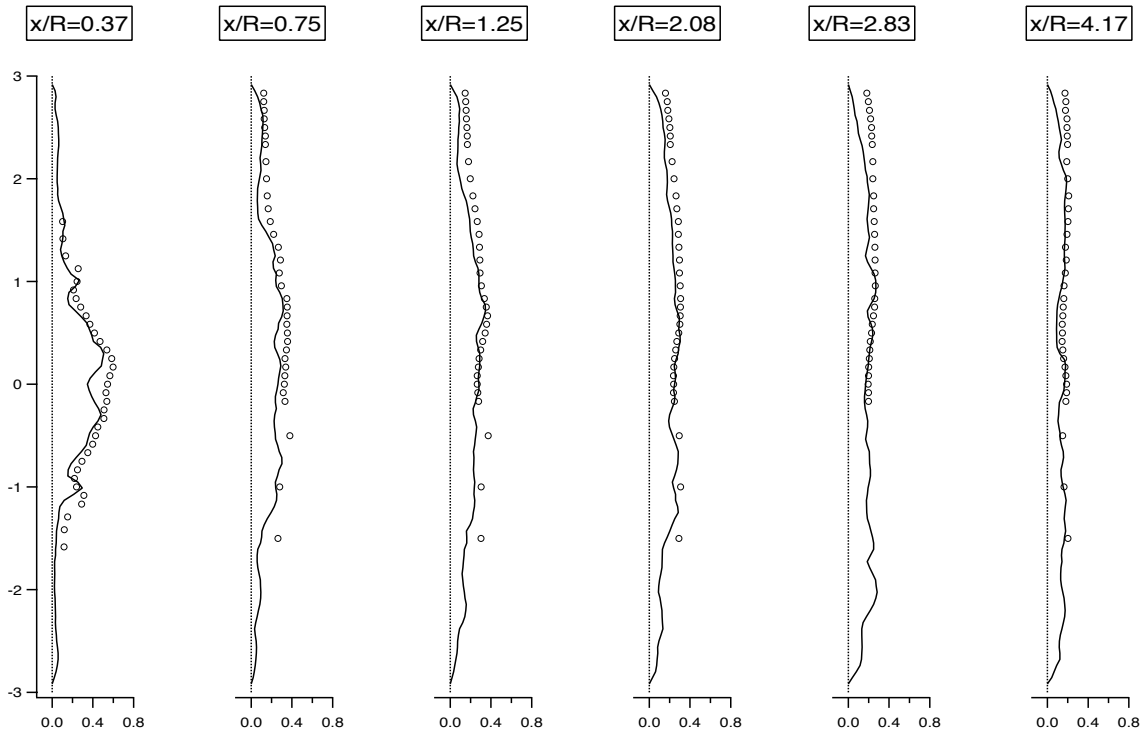

Figure 4.9: Cold flow swirling velocity fluctuations (W'/U_{bulk}). ○ LDV; —— LES.

section by the presence of a coherent structure.

An additional quantity which can be extracted directly from this compressible LES is the RMS pressure P', both in the chamber and on its walls. Fig. 4.10 shows that the largest pressure oscillations are found in front of the axial swirler outlet. Fairly high pressure levels ($2500Pa$) are observed inside the combustor at the swirler outlet but they do not propagate to the walls. Most of these pressure oscillations are due to the precessing vortex described in the next section.

4.3.2 Unsteady flow analysis

Swirling flows can exhibit a very large range of topologies, mainly depending on the swirl number (see the review on vortex breakdown in (Lucca-Negro and O'Doherty 2001)). For high values of the swirl number, the central recirculation zone may oscillate at a given frequency. This phenomenon is often reffered to as precessing vortex core (PVC). Fig. 4.11 shows the topology of a precessing vortex core. The vortex aligned with the axis of the chamber (due to the swirl) breaks down at the stagnation point S in a spiral form. In the present regime, the flow inside the spiral is recirculated. The entire structure rotates around the axis of the chamber, causing large perturbations.

The present LES captures this phenomenon: on the burner axis, at point A1 (Fig. 4.3), the velocity component W oscillates with time (Fig. 4.12) at a frequency $f_{\mathrm{LES}} = 280$ Hz. If the flow were axisymetric, W would be zero on the axis of the burner. The computed strouhal number $St = (2Rf_{\mathrm{LES}})/U_{bulk} = 0.63$ is typical of swirling flows (Gupta et al. 1984). The value of f_{LES} is also very close to that obtained experimentally at ITS: $f_{\mathrm{exp}} = 260$ Hz.

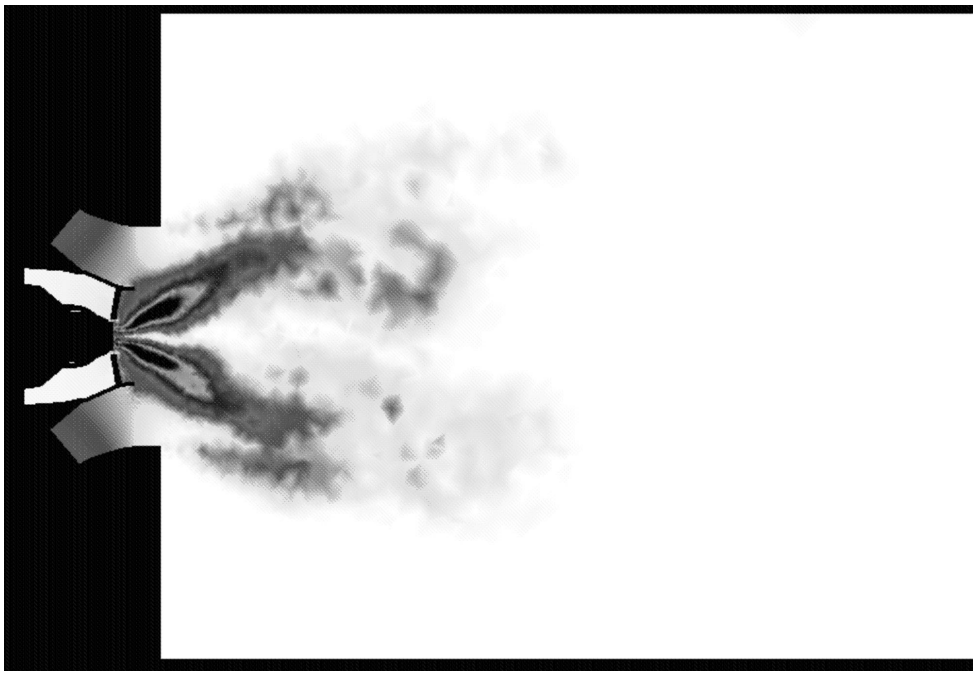

Figure 4.10: RMS pressure fluctuations P' in a longitudinal cut for the cold flow (Pa).

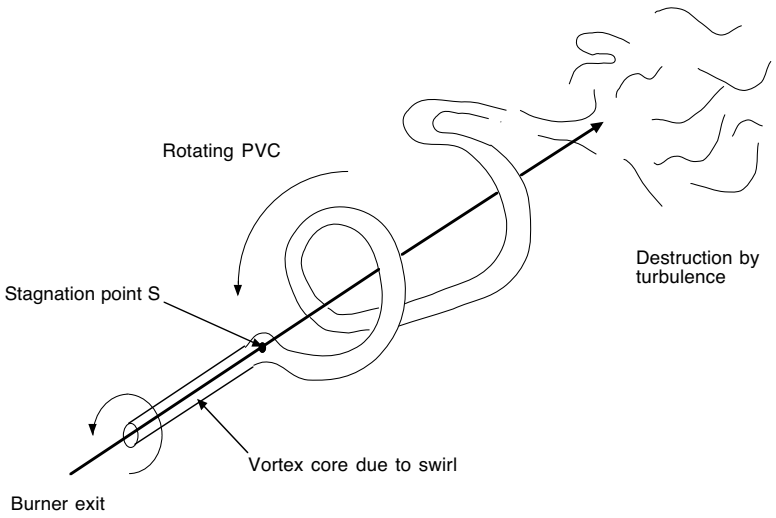

Figure 4.11: Topology of a precessing vortex core (PVC).

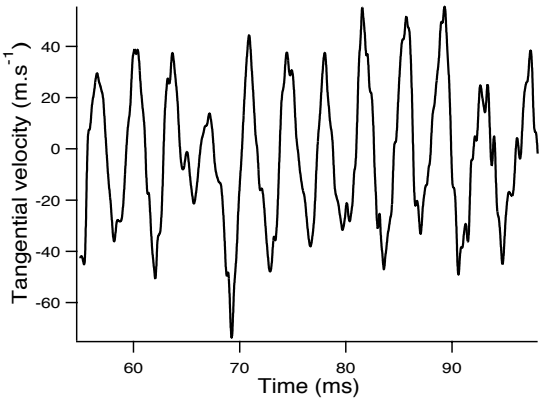

Figure 4.12: Cold flow: W velocity at point A1 (Fig. 4.3).

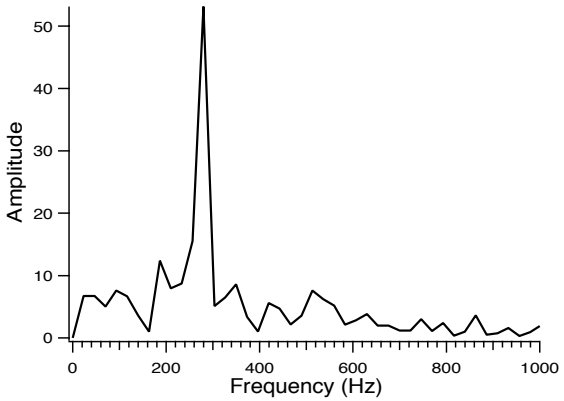

Figure 4.13: Cold flow: Fourier transform of W velocity signal at point A1.

Note that the LES gives an additional information on the temporal evolution of the spiral: the sense of winding of the spiral and the sense of rotation of the whole spiral, as a structure, is that of the surrounding swirling flow. This finding is coherent with other observation (Dellenback et al. 1988, Guo et al. 2001): at strong levels of swirl, the PVC rotates in the same direction as the flow. Fig. 4.14 is an instantaneous visualisation of the PVC in the cold flow.

4.4 Reacting flow results in configuration 1

4.4.1 Ignition methodology

Igniting an LES computation raises problems which are very similar to igniting a real experiment: too strong ignition can lead to oscillations or flasback while too weak ignition will fail. In the present case, fresh premixed gases (equivalence ratio $\phi = 0.5$) are injected through the diagonal and the axial swirler. Both flows, coming from the compressor in the actual gas turbine, enter the combustion chamber of the ITS burner after being preheated electrically to a temperature $T = 673$K. As the actual ignition process (produced by a spark in the real experiment) is not described here, the chemical reaction is numerically started by filling the combustion chamber with hot fully burned gases. Note however that the pressure increases by 25 % and the exit velocity Mach number goes up to 0.4 in the outlet contraction during the transient ignition phase (Selle et al. 2002).

4.4.2 Unsteady flow analysis

After a few flow-through times in the combustion chamber, the computation stabilizes and mean values converge. An example of the reacting flow field observed after this initial phase is displayed in Fig. 4.15: the temperature isosurface at $T = 1000$K shows the topology of the flame surface. Pockets of fresh gases are periodically shed from the main flame zone and burn downstream. A central core of hot gases is stabilized along the burner axis by the recirculation zone induced by swirl: this core is attached to the face of the axial swirler (Fig. 4.16). The field of axial velocity, normalized by U_{bulk}, is displayed in Fig. 4.17 with isocontours of heat release.

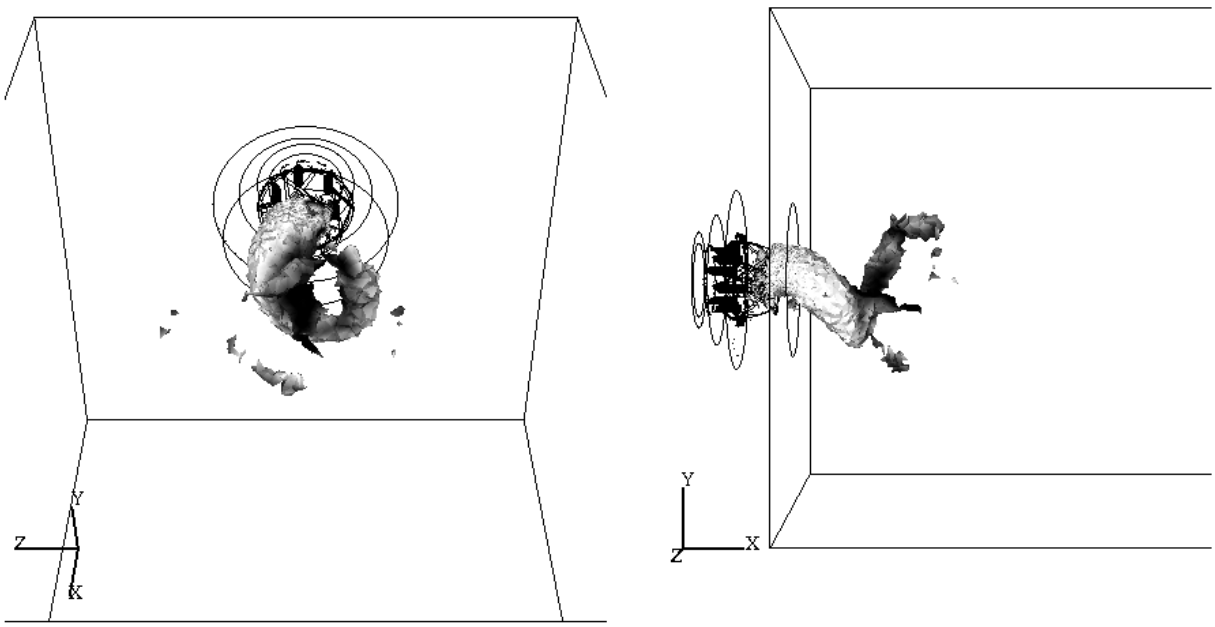

Figure 4.14: Visualisation of the PVC structure by a Pressure iso-surface.

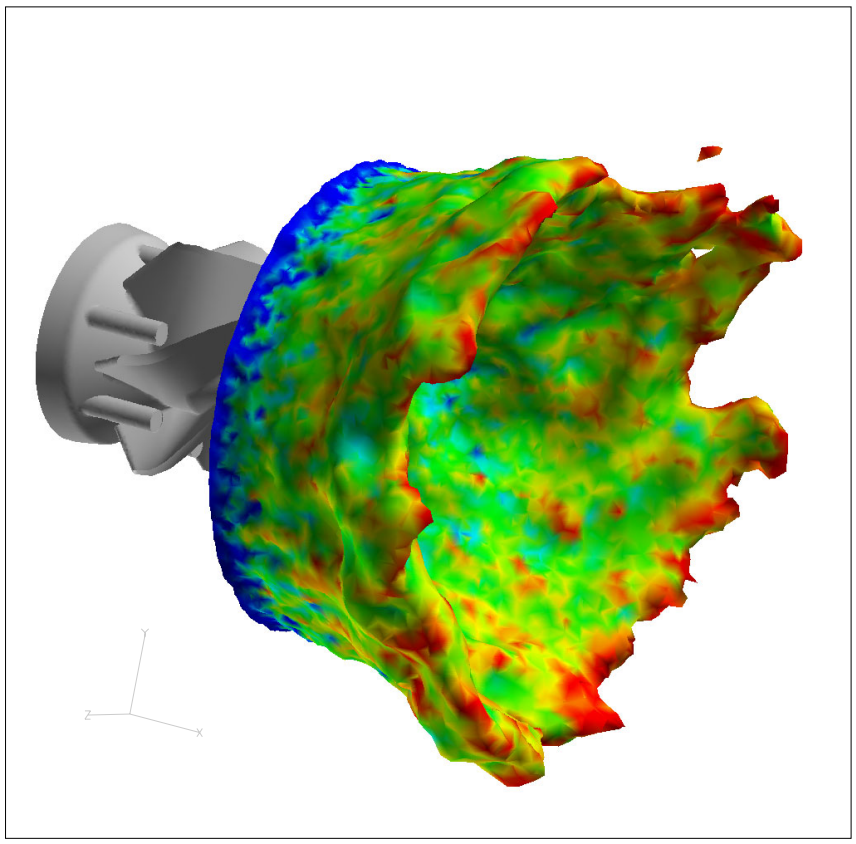

Figure 4.15: Axial swirler vanes and isosurface of temperature ($T = 1000$K) colored by velocity modulus (see full animation at http://www.cerfacs.fr/cfd/FIGURES/MOVIES/flame-ITS.mov).

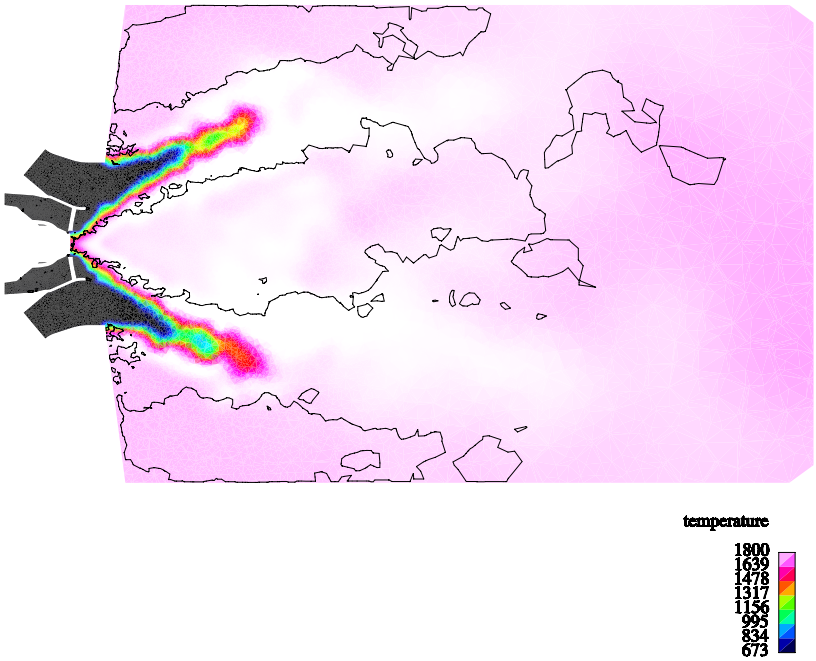

Figure 4.16: Instantaneous temperature field and contours of zero axial velocity in a longitudinal cut of the burner.

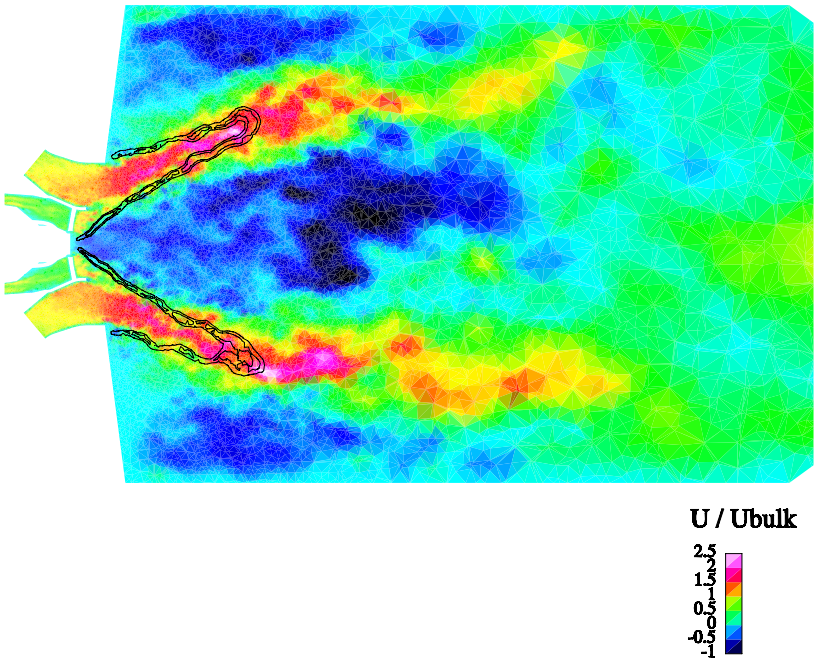

Figure 4.17: Instantaneous axial velocity field and contours of reaction rate in a longitudinal cut of the burner.

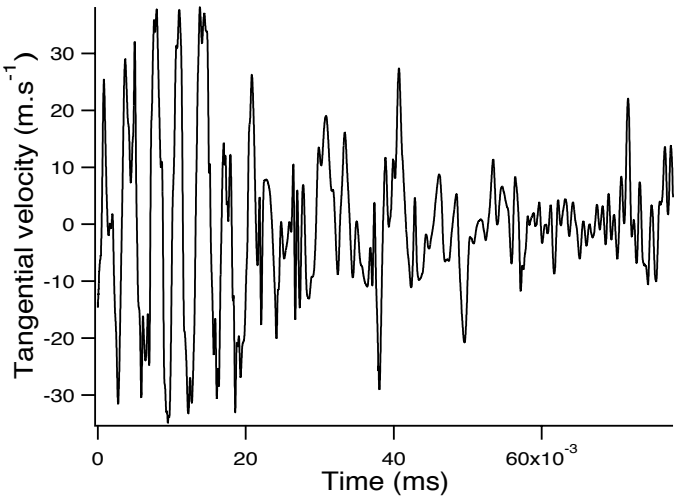

Figure 4.18: Reacting flow: W velocity signal at point A1 (Fig. 4.3) after ignition.

A specific feature of the reacting case is that the PVC structure evidenced in the cold flow cases disappears when combustion is turned on. Fig. 4.18 is a record of the velocity in the horizontal central plane (W) at point A1 (Fig. 4.3) after ignition. The velocity signal oscillates around zero as the core of the recirculation zone moves around the axis of the combustion chamber. After a few periods, the PVC motion vanishes. This observation obtained from LES data is confirmed by experimental results.

4.4.3 Averaged fields

Mean LES results (——) can be directly compared to experimental data (∘). Fig. 4.19 shows the measurements conducted only in one half of the combustion chamber. Mean temperature profiles obtained from LES are compared to experimental data in Fig. 4.19. The thickness of the turbulent flame brush is slightly underestimated (see $x/R = 0.7$ in Fig. 4.19). However, the agreement between LES and experimental data is good, and quantities which are important for the turbine design, are well reproduced:

- the length of the flame is well predicted,
- the burnt gas temperature is very slightly overpredicted by the LES, mainly due to the non-adiabaticity of the experiment, while the LES assumes adiabatic walls.

Fig. 4.20 is the iso-surface $T = 1000K$ of the mean solution. The wakes of the six blades of the axial swirler are clearly visible, showing the necessity of meshing the axial swirler.

4.4.4 Acoustic analysis

The unsteady pressure fields in this configuration can be obtained by two methods:

- (1) the LES fields can be post processed. Since the LES code is compressible, the unsteady field will reveal any existing acoustic mode. In this aspect, LES could provide all information and avoid using any acoustic tool: unfortunately, it is much too expensive to do so.

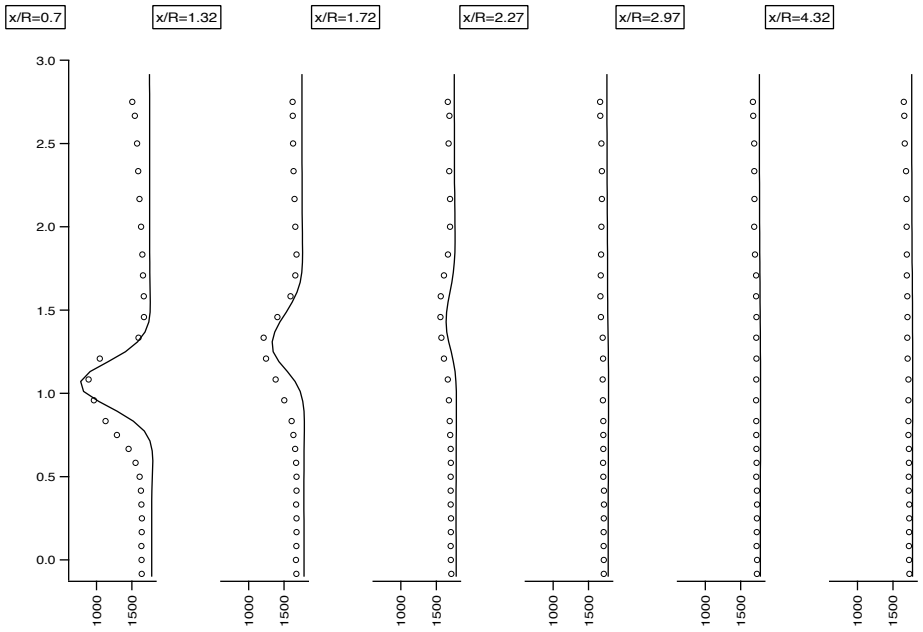

Figure 4.19: Reacting flow mean temperature (K).

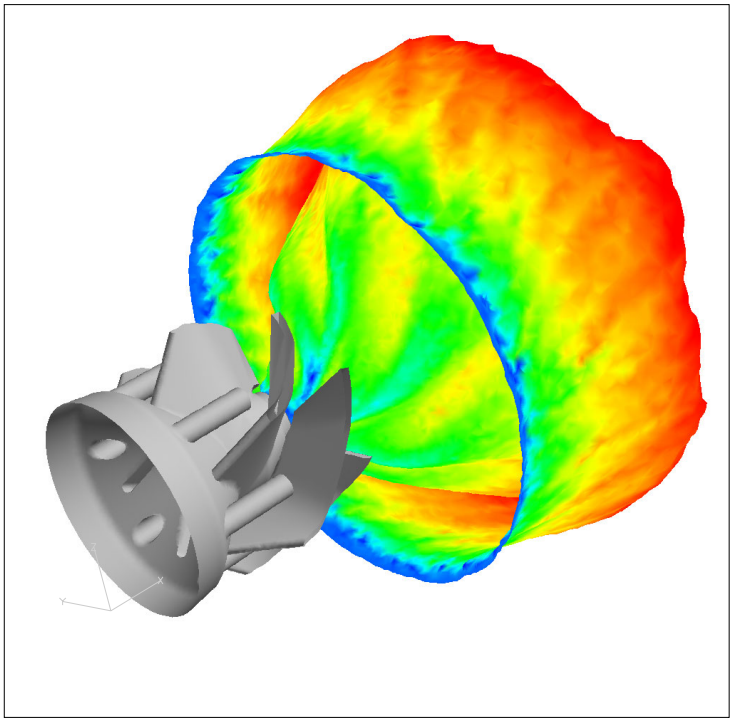

Figure 4.20: Mean flow. Axial swirler vanes and isosurface of temperature ($T = 1000$K) colored by velocity modulus.

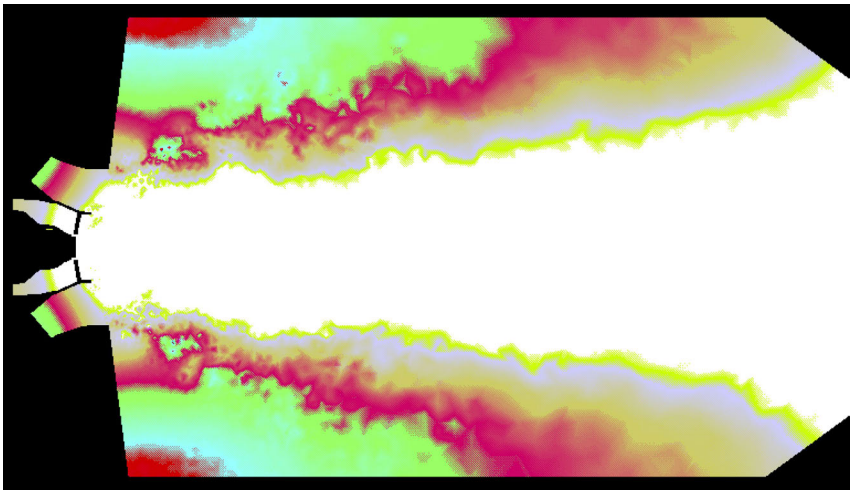

Figure 4.21: RMS pressure fluctuations P' in a longitudinal cut for the hot flow (Pa).

- (2) A three-dimensional Helmholtz tool such as AVSP described in Section 3.2 can be used on the mean temperature fields given by the LES to determine the eigenmodes of the burner.

Both methods have been used here and are presented below.

Acoustic field revealed by LES

Post processing the LES provides the field of the pressure fluctuations P'. Analyzing this field in a longitudinal cut reveals a very important difference between cold and reacting flow: the pressure fluctuations observed in the cold flow (see Fig. 4.10) in front of the axial swirler disappear when combustion is turned on (Fig. 4.21). This is consistent with the suppression of the PVC when combustion is started: the cold flow unsteady pressure field is dominated by the presence of the PVC while the reacting flow inhibits the PVC.

Another very important point revealed by LES is the existence of a coherent acoustic mode in the chamber induced by combustion: plotting P' on the walls of the combustion chamber (Fig. 4.22) shows that an acoustic mode of the chamber is now excited. This mode has a transverse structure: which seems to be that of a quarter-wave length in the x direction, and half-wave length in both cross directions. A direct examination of animated unsteady pressure fields shows that the mode is actually turning around the main chamber axis. This can be demonstrated by plotting time signals at adequate points: Fig. 4.23 displays pressure versus time for four points C_1, C_2, C_3 and C_4 located in the corner recirculation zones (see Fig. 4.2). The phase difference between consecutive pressure tracers is $\pi/2$: this indicates that the acoustic mode is rotating aroud the main burner axis. The frequency of this mode is 1200 Hz.

Acoustic field revealed by a Helmholtz code

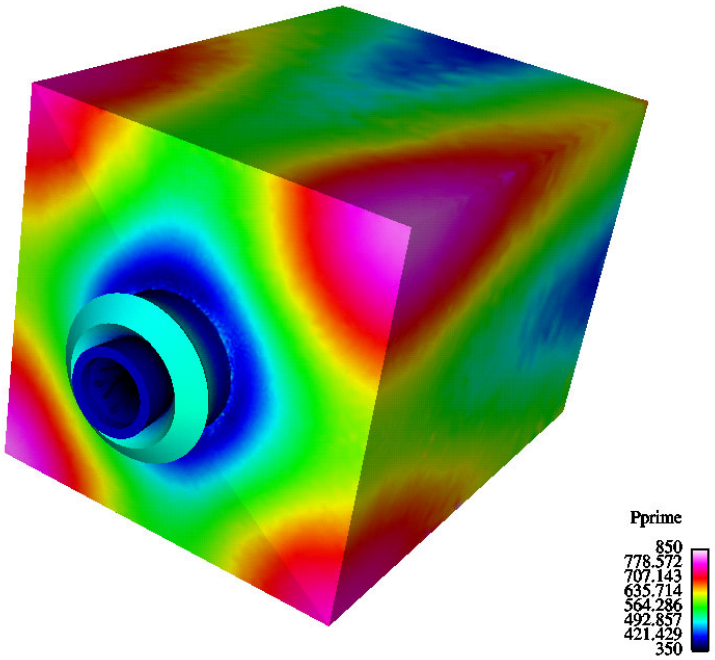

Figure 4.22: RMS pressure fluctuations P' on the walls of the chamber for hot flow (Pa) obtained by averaging LES data.

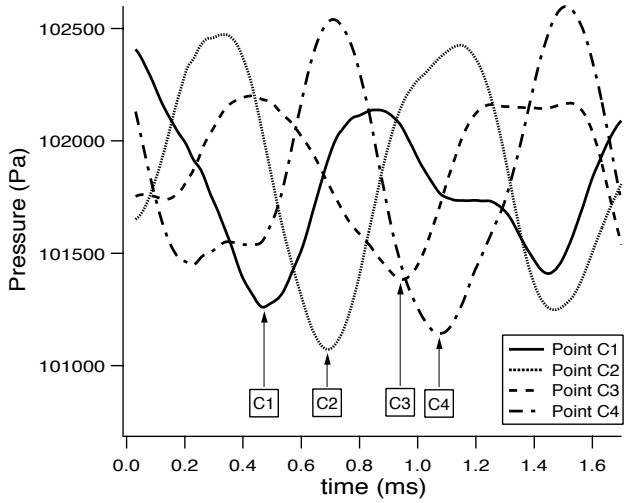

Figure 4.23: Pressure signal versus time in the corner recirculation zones of the chamber. A rotating acoustic mode is evidenced (see full animation at http://www.cerfacs.fr/cfd/FIGURES/MOVIES/P_traces_trans-ITS.mov).

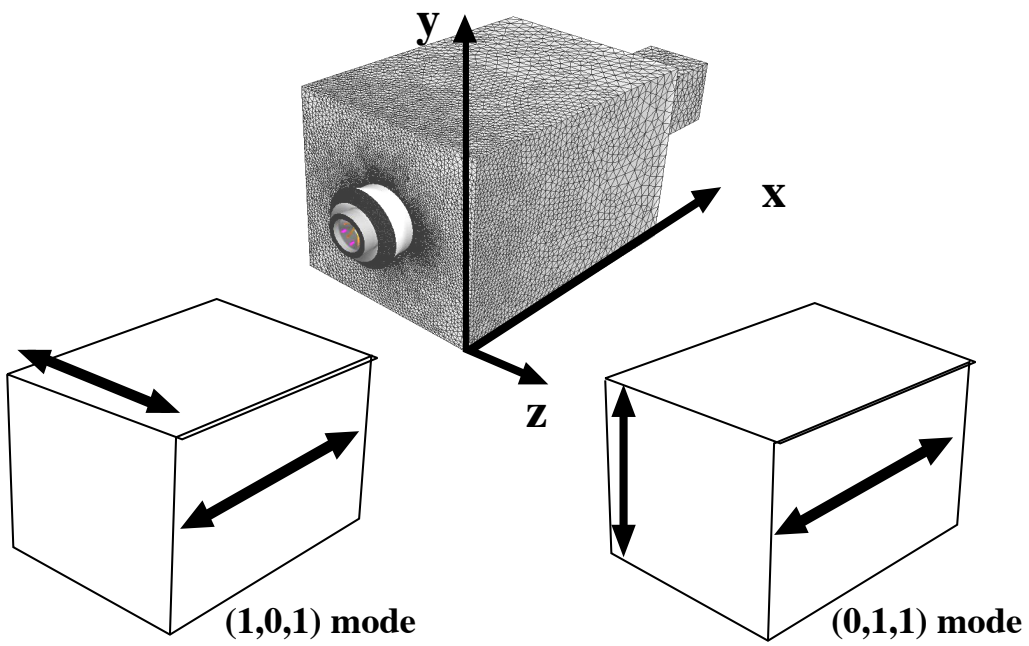

Figure 4.24: Structure of the two transverse modes (1,0,1) and (0,1,1).

The mean temperature field and the chamber geometry can be fed into a Helmholtz code to obtain all acoustic eigenmodes of the cavity. Hard walls ($u' = 0$) are assumed for all walls. The inlet and outlet sections correspond to open boundaries where p' is set to zero. Table 4.1 shows the list of the eigenmodes and their structure.

Mode number	Mode name	Frequency (Hz)
(1,0,0)	first longi in x	314
(2,0,0)	second longi in x	869
(1,0,1)	first transverse in z / first longi in x	1228
(1,1,0)	first transverse in y / first longi in x	1228
(3,0,0)	third longi in x	1466
(2,0,1)	first transverse in z / second longi in x	1493
(2,1,0)	first transverse in y / second longi in x	1493
(1,1,1)	first transverse in y, first transverse in z, first longi in x	1705

Table 4.1: Helmholtz code (AVSP) results for configuration 1: list of modes and frequencies

The (1,0,1) and the (1,1,0) modes are of special interest: their frequencies are equal because the chamber section is square. Their structure is displayed in Fig. 4.24 where the arrow indicates the direction of non homogeneity. The frequency of this degenerated mode (1228 Hz) also matches the frequency observed in LES: 1200 Hz. But they correspond to transverse modes and not to a rotating mode: how can this result be compatible with the LES observation ? Actually, since these two modes have the same frequency, they can be combined. Simply adding them and shifting the second one by ninety degrees leads to a rotating mode which is extremely similar to the pattern obtained by LES. Snapshots of pressure at four successive instants are plotted for this mode in Fig. 4.25.

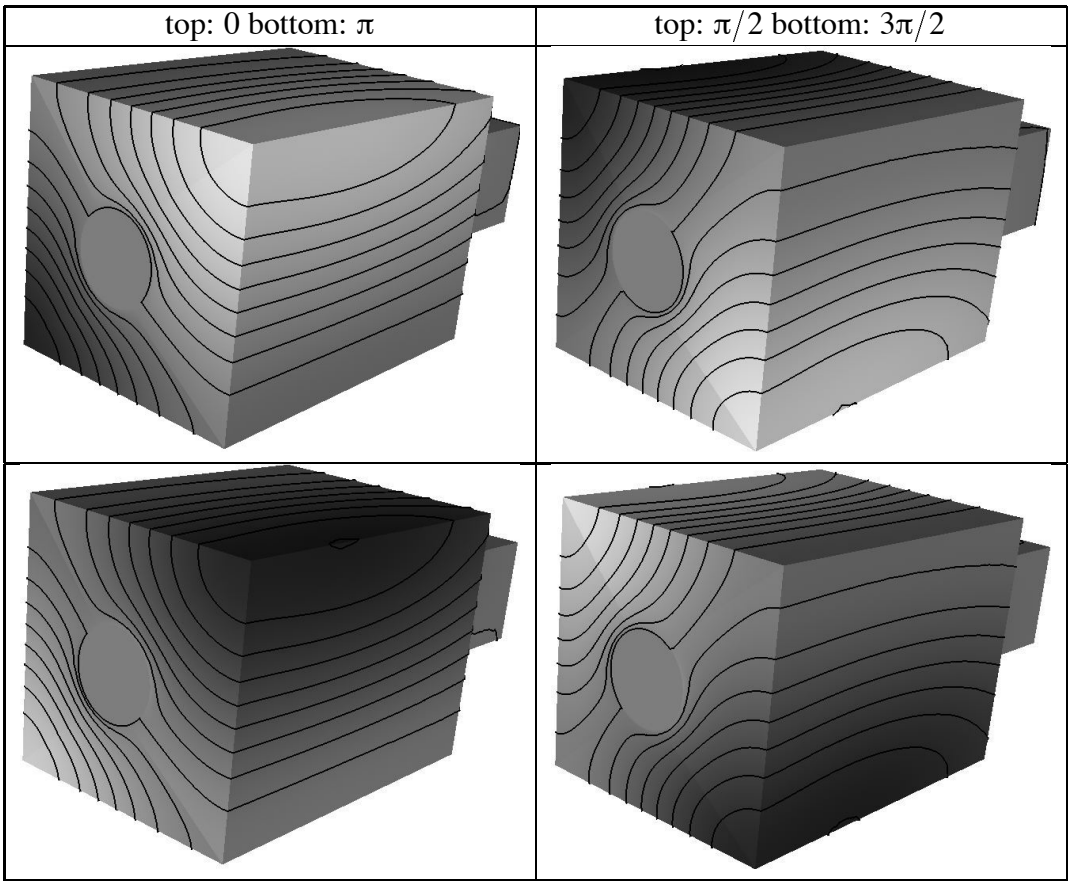

Figure 4.25: Instantaneous pressure signals at four phases (0, $\pi/2$, π and $3\pi/2$) separated by a quarter period of the turning 1228 Hz mode. Dark zones: maximum pressure.

Averaging these fields over time leads to the RMS pressure field displayed in Fig. 4.26 which is very similar to Fig. 4.22. The Helmholtz code brings here a precious simple information: the turning mode evidenced in the LES is nothing else than the combination of the two first transverse modes of the combustion chamber shifted by ninety degrees. WHY these two modes combine in such a way remains an open question. It can not be addressed without introducing an active flame into the Helmholtz solver as discussed in Section 3.2.

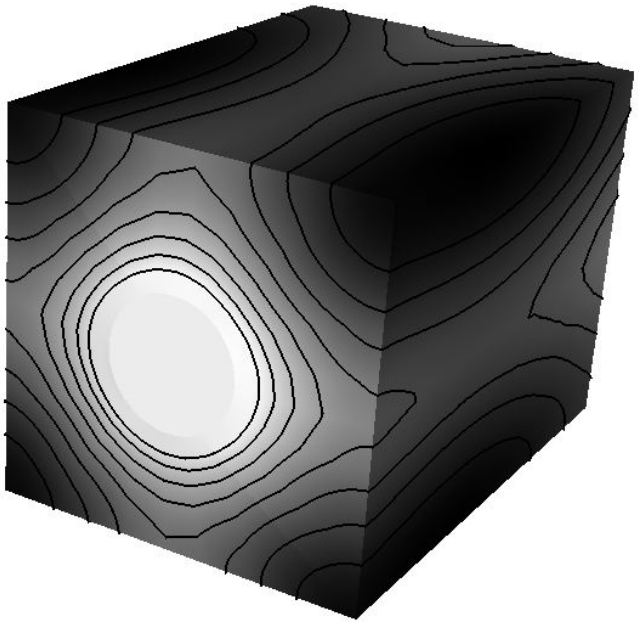

Figure 4.26: RMS pressure field on the walls for the 1228 Hz mode obtained by the Helmholtz code. To compare with the LES result given in Fig. 4.22.

Chapter 5

Application to configuration 2

5.1 Geometry and regime in configuration 2

The second burner is a swirled injector of smaller size which could fit for example in an helicopter turbine. Its geometry is displayed in Fig. 5.1. Swirl is produced here by tangential injection. A central hub is used to stabilize the swirl and the flame. The swirling section is fed with air through a plenum chamber. In the experiment, methane is injected through holes located in the swirler but for the present computations, perfect premixing has been assumed.

Experiments have been performed at DLR and include velocity measurements for the cold flow as well as a study of various combustion regimes and instabilities.

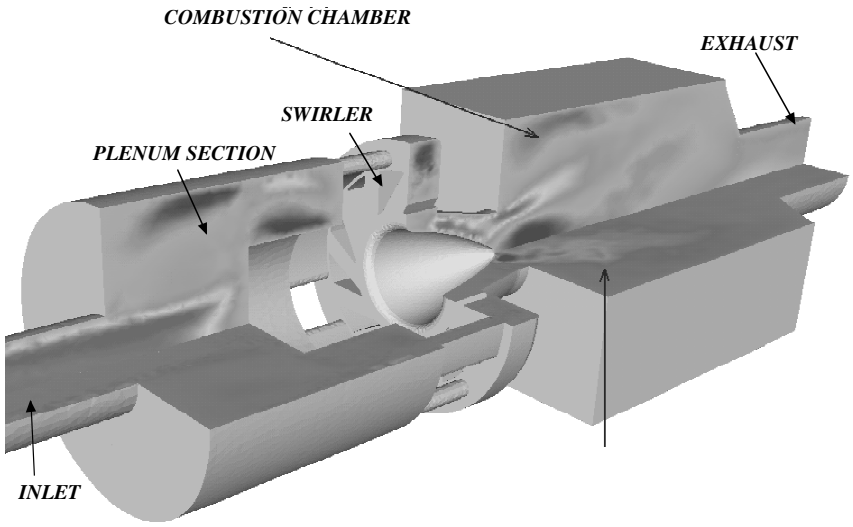

Figure 5.1: Burner and combustion chamber for configuration 2.

5.2 Inlet conditions in configuration 2

For this burner, the critical question of boundary conditions is avoided by computing everything upstream and downstream of the burner: even a part of the outside atmosphere at the

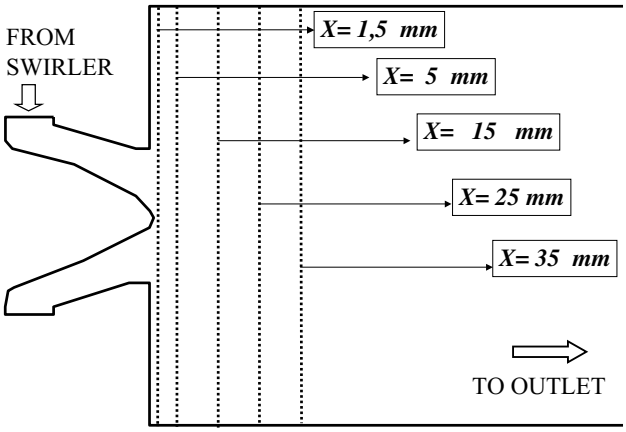

Figure 5.2: Location of cuts for velocity profiles comparisons in configuration 2.

chamber exhaust is meshed to avoid having to specify a boundary condition at the chamber outlet (Fig. 5.1).

The expected precision of the solver in terms of acoustic waves interacting with the outlet of the chamber is much better since this section is not a boundary condition but a part of the computational domain. This is also a very interesting test for LES in which the boundary conditions cannot be blamed if the comparison with experimental data is not good.

5.3 Non reacting flow in configuration 2

5.3.1 Average fields

Average velocity profiles have been compared at various sections of the combustion chamber (Fig. 5.2). The averaging time for LES is 100 ms corresponding to 15 flow-through times in the combustion chamber at the bulk velocity. Data compared for LES and experiments are :

- Average axial (Fig. 5.3) and azimuthal (Fig. 5.5) velocities in 5 sections. These profiles are averaged over time (no spatial averaging in directions of homogeneity).
- RMS axial (Fig. 5.4) and azimuthal (Fig. 5.6) velocities in the same sections.

The comparison of all profiles shows an excellent agreement for all quantities: the mean velocity is correctly predicted as well as the length of the central recirculation zone (Fig. 5.3) . The swirl levels are also very good (Fig. 5.5): considering that this computation has absolutely no inlet boundary condition which can be tuned to fit the velocity profiles, this confirms the capacity of LES in such flows. The profiles of RMS velocities obtained experimentally by LDV and numerically by LES, both for axial (Fig. 5.4) and azimuthal (Fig. 5.6) are also very close. The level of RMS fluctuations is very high on the axis, close to the mouth of the burner (of the order of 20 m/s at $x = 1.5$ mm both for LDV and LES. This is again the sign of the presence of a strong Precessing Vortex Core in this region as discussed in the next section. This also explains why RANS codes would have difficulties predicting such a flow which is dominated by a large structure while LES performs very well in this case.

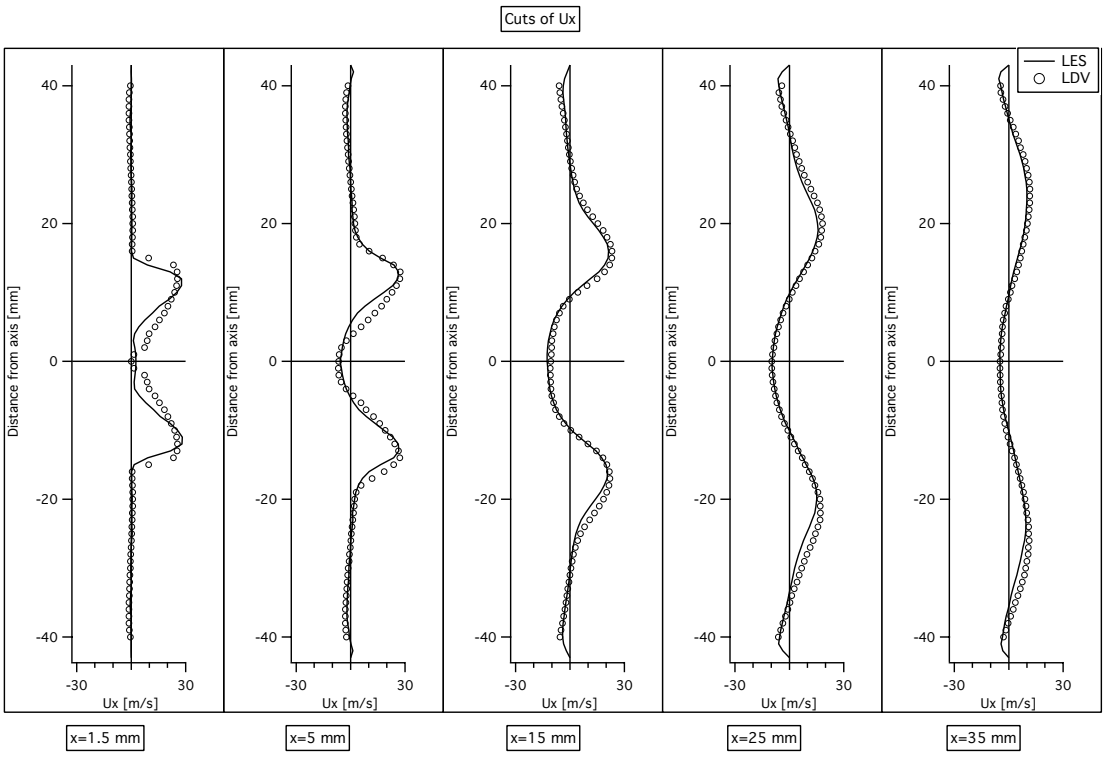

Figure 5.3: Average axial velocity profiles in configuration 2. ○ LDV; ——LES.

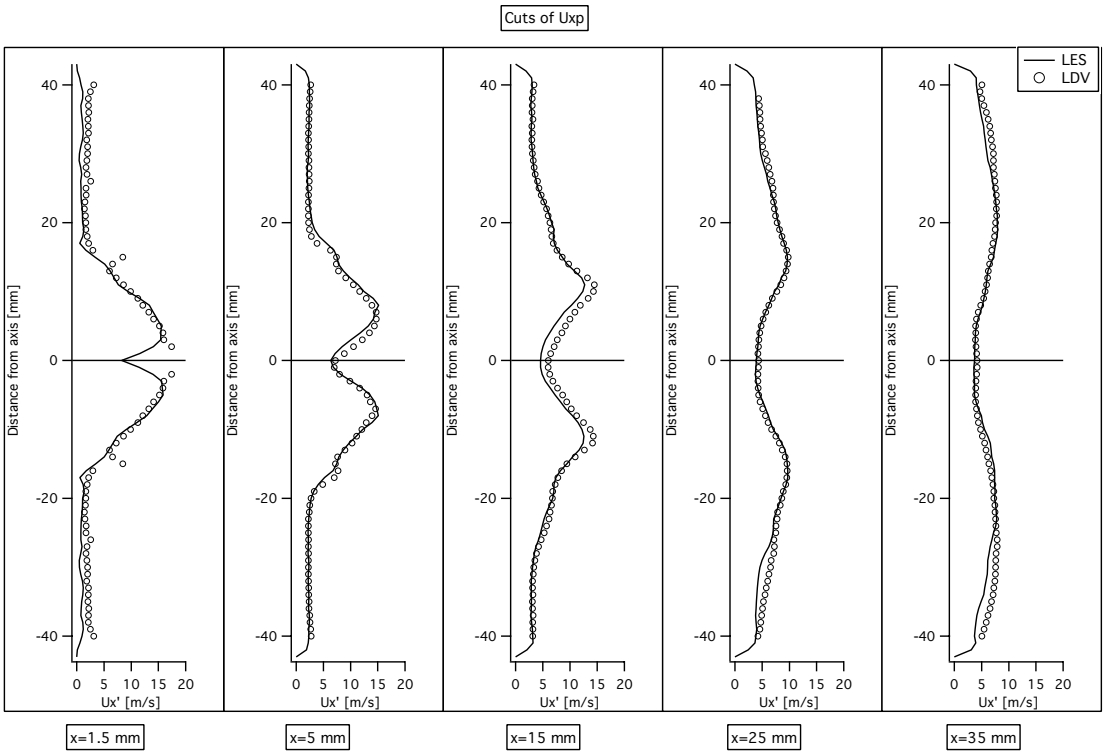

Figure 5.4: RMS axial velocity profiles in configuration 2. ○ LDV; ——LES.

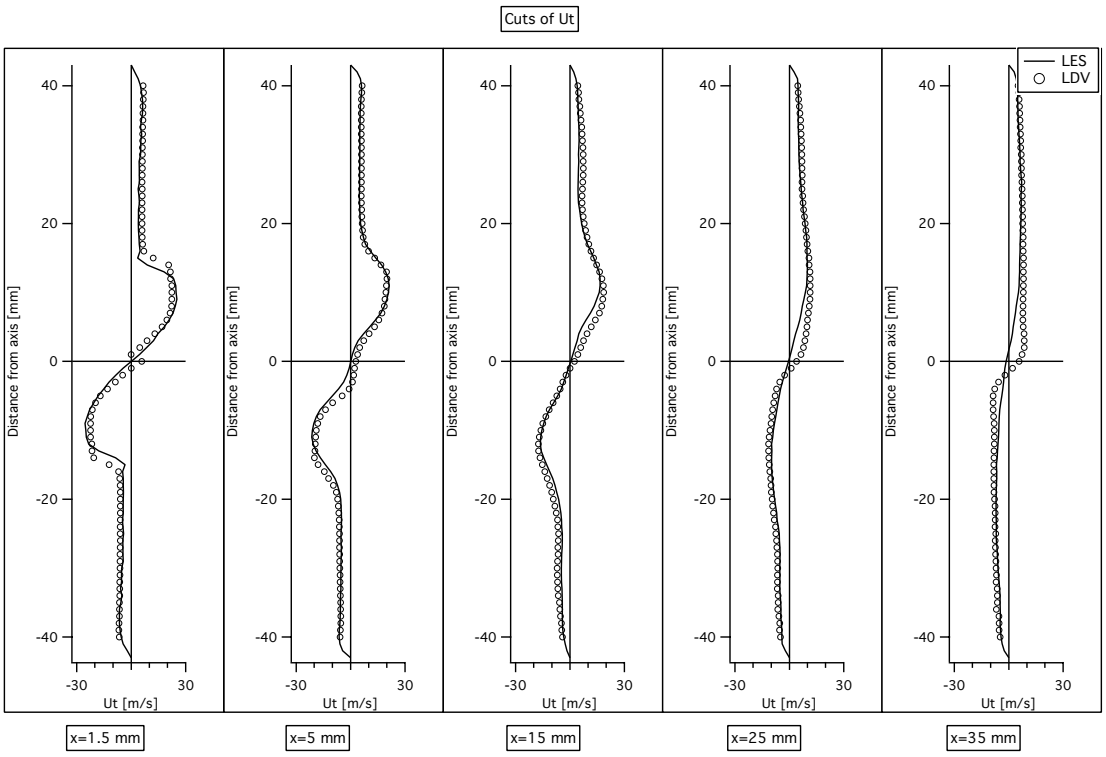

Figure 5.5: Average azimuthal velocity profiles in configuration 2. ○ LDV; ——LES.

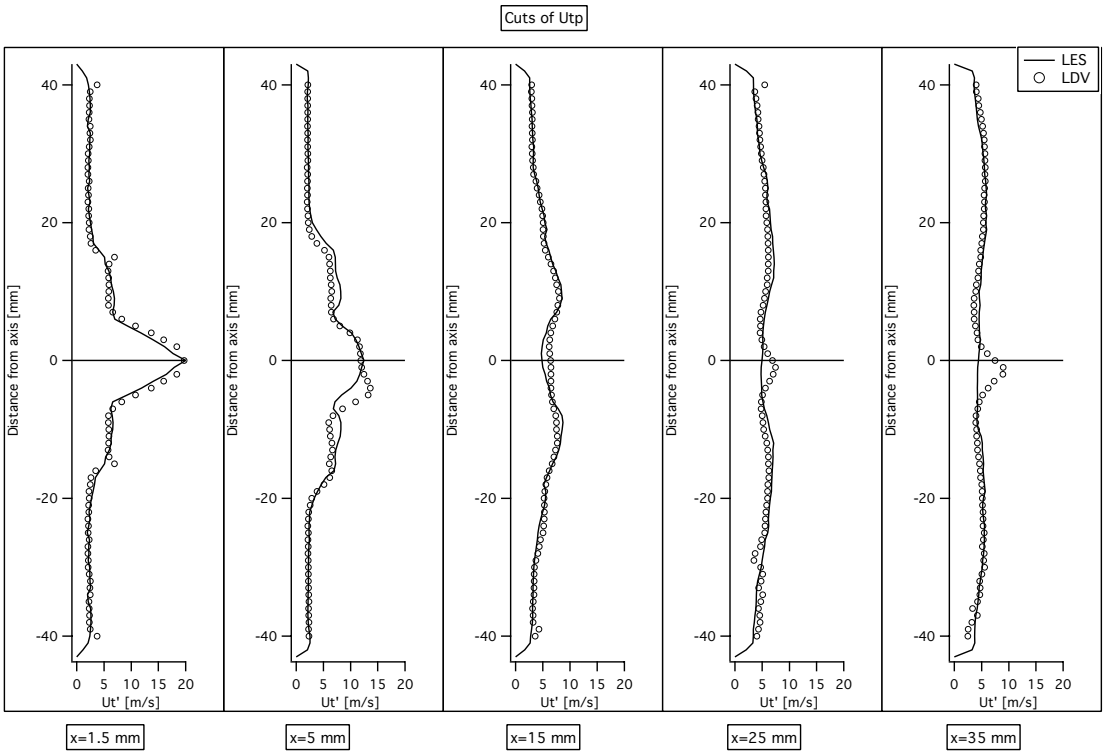

Figure 5.6: RMS azimuthal velocity profiles in configuration 2. ○ LDV; ——LES. .

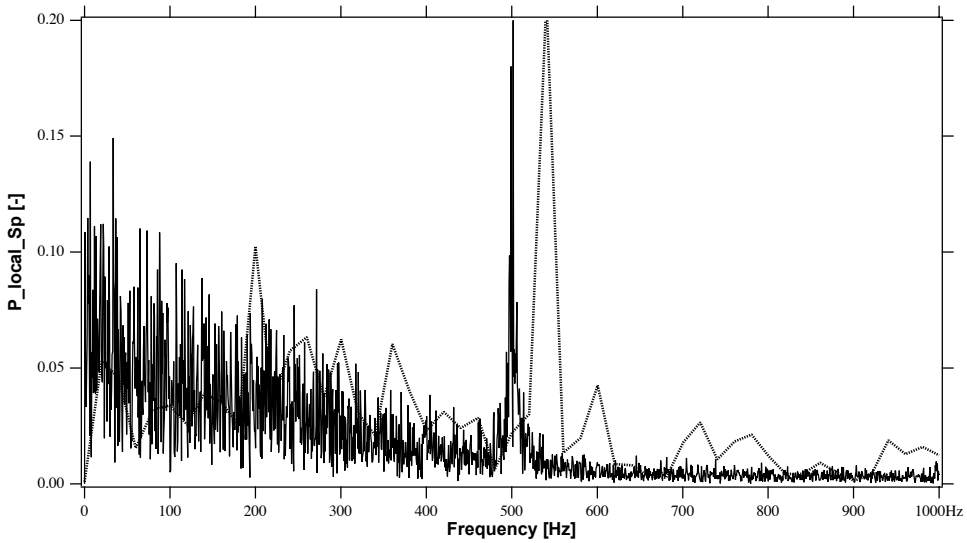

Figure 5.7: Spectra inside the chamber for configuration 2. The LES (dotted line) signal is a wall pressure signal while the experimental data (solid line) is obtained with LDV. Results have been scaled for comparison.

5.3.2 Unsteady non reacting flow

This strongly swirled flow also exhibits a characteristic vortex core visualized in Fig. 5.8. The frequency of this PVC is 520 Hz, corresponding to a Strouhal number based and on the burner mouth R and on the bulk velocity $U_b = \dot{m}/(\rho\pi R^2$ of 0.8, slightly larger than values found in the litterature for simple swirling flows. Both the LES and the measurements performed inside the chamber reveal peaks which exhibit very close frequencies (520 for the LES and 505 Hz for the experiment (Fig. 5.7).

This PVC is obviously the source of the RMS velocitites evidenced in Fig. 5.4 and Fig. 5.6. It also creates a region of unsteady pressure visualized in Fig. 5.9.

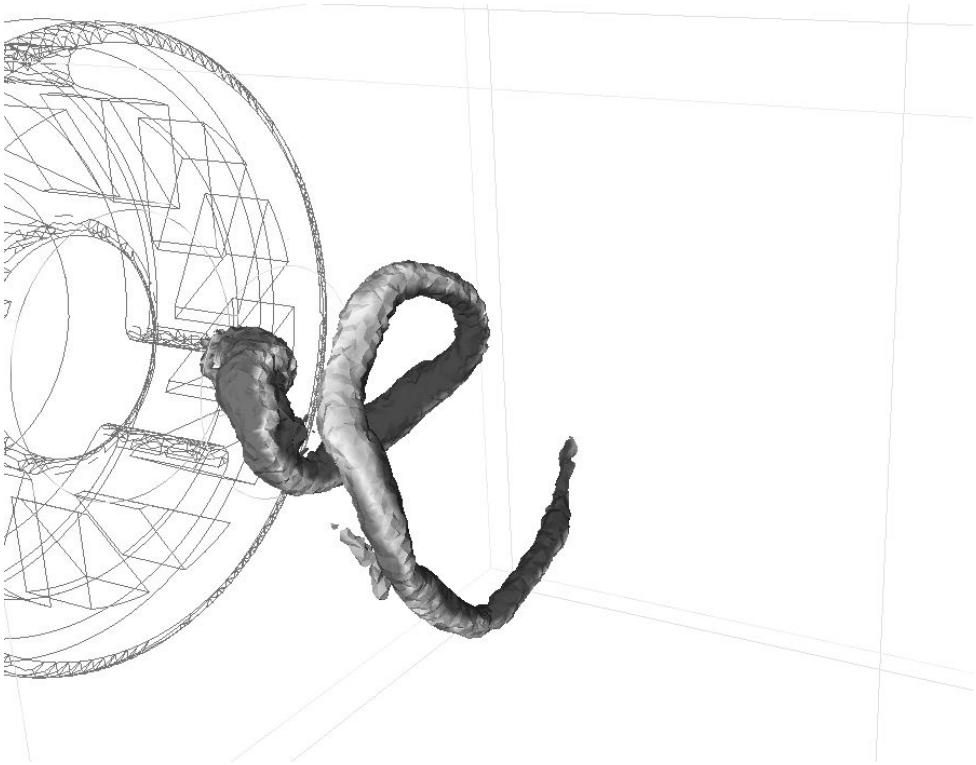

Figure 5.8: Visualization of the PVC mode in configuration 2 using an isosurface of low pressure.

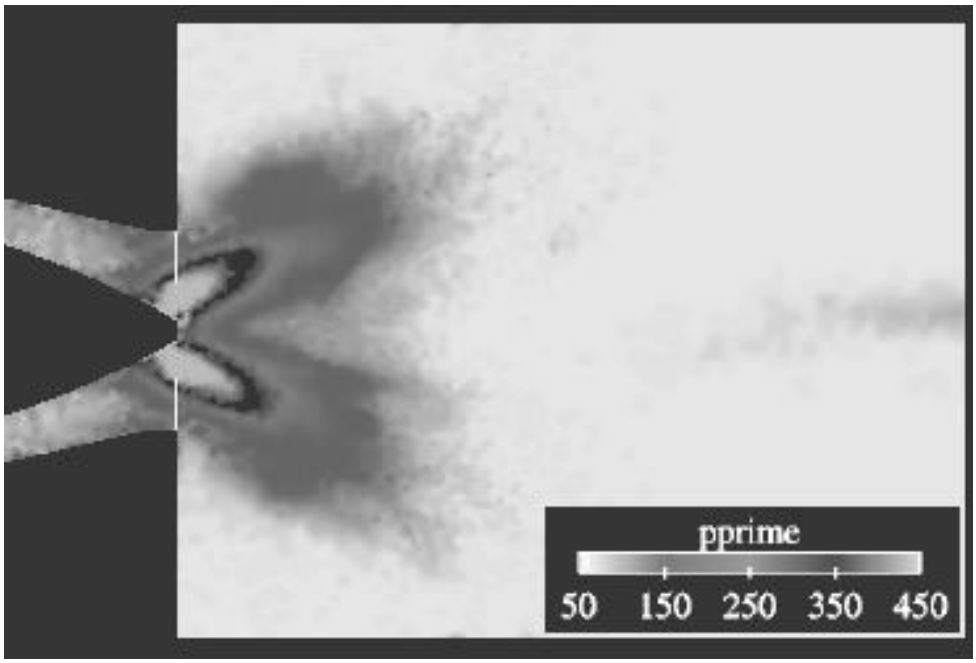

Figure 5.9: Field of RMS pressure fluctuations in the central plane of the combustor for configuration 2 (non reacting case).

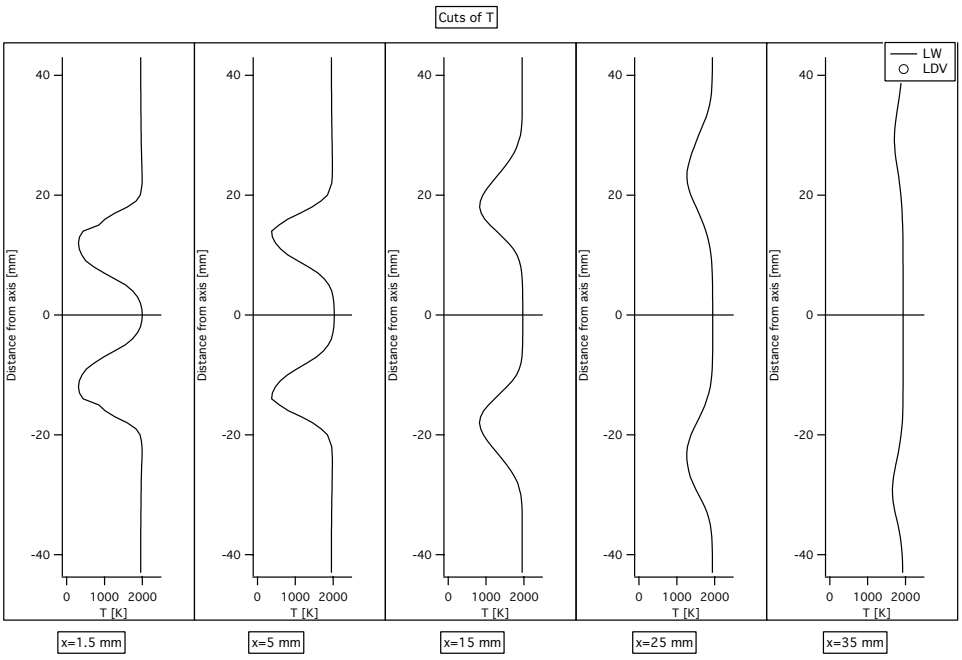

Figure 5.10: Field of mean temperature in the central plane of the combustor for configuration 2 (LES data).

5.4 Reacting flow in configuration 2

The reacting case presented here corresponds to an equivalence ratio of 0.75, an air flow rate of 12 g/s and a power of 27 kW. When combustion is activated in configuration 2 for this case, a steady regime is found but this regime presents self-excited oscillations.

5.4.1 Average fields

The average field of temperature (Fig. 5.10) reveals a very compact flame located close to the burner mouth. No comparison is possible with experiments because temperatures were not measured.

The velocity fields, however, were measured and are presented in Fig. 5.11 (mean axial velocity), 5.12 (RMS axial velocity), 5.13 (mean tangential velocity) and 5.14 (RMS tangential velocity). Radial velocities were also measured but not presented here although they comapre very well with LES results. The overall agreement between mean LES results (solid lines) and experimental data (symbols) is very good. The LES captures both the mean values and the fluctuations very precisely. Note again that no boundary condition can be tuned to obtain this result since the computation domain starts in the plenum and ends in the atmosphere.

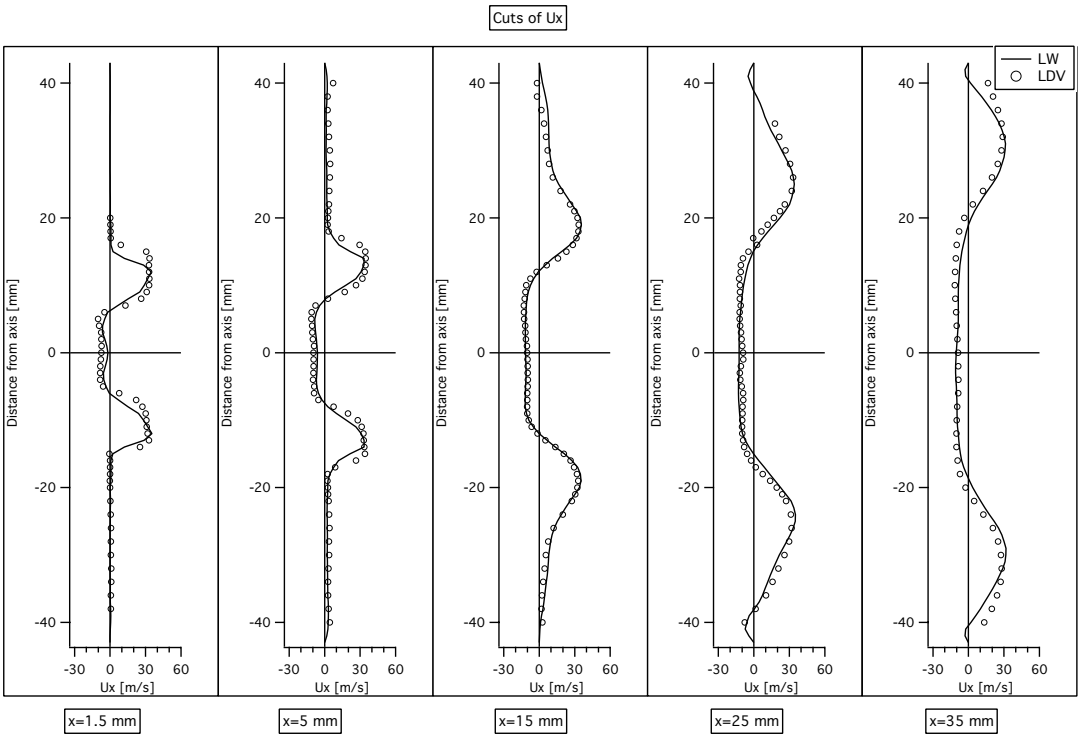

Figure 5.11: Mean axial velocity in the central plane for configuration 2. ○ LDV; ——LES.

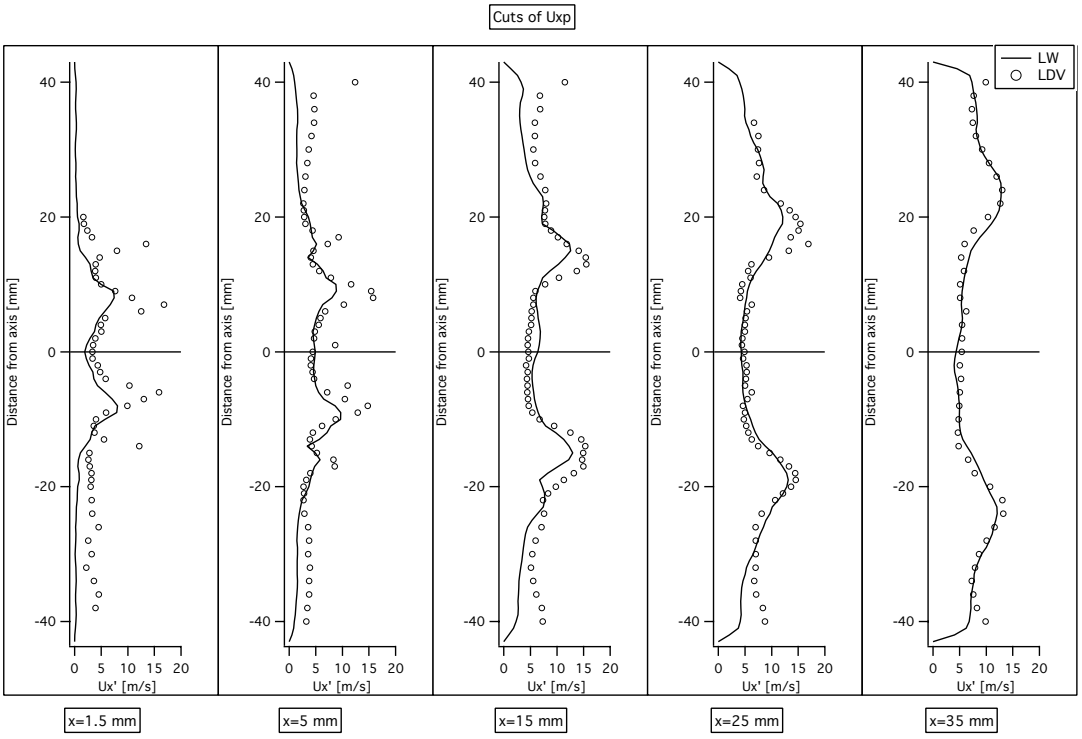

Figure 5.12: RMS axial velocity in the central plane for configuration 2. ○ LDV; ——LES.

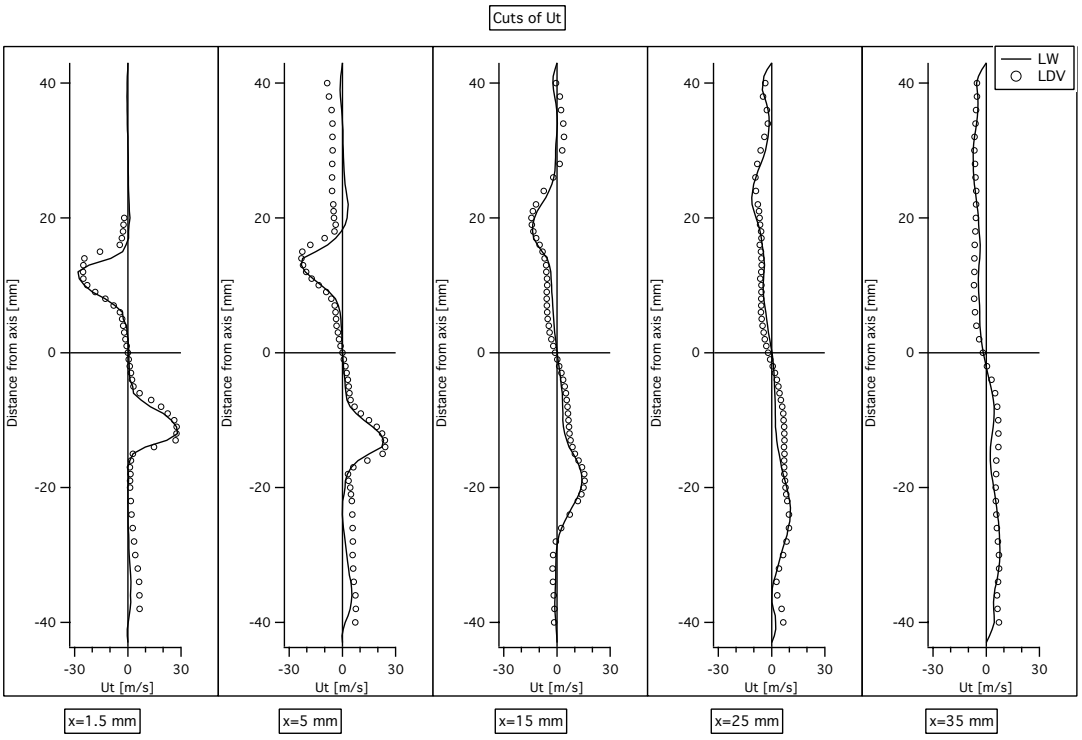

Figure 5.13: Mean tangential velocity in central plane for configuration 2. ○ LDV; ——LES.

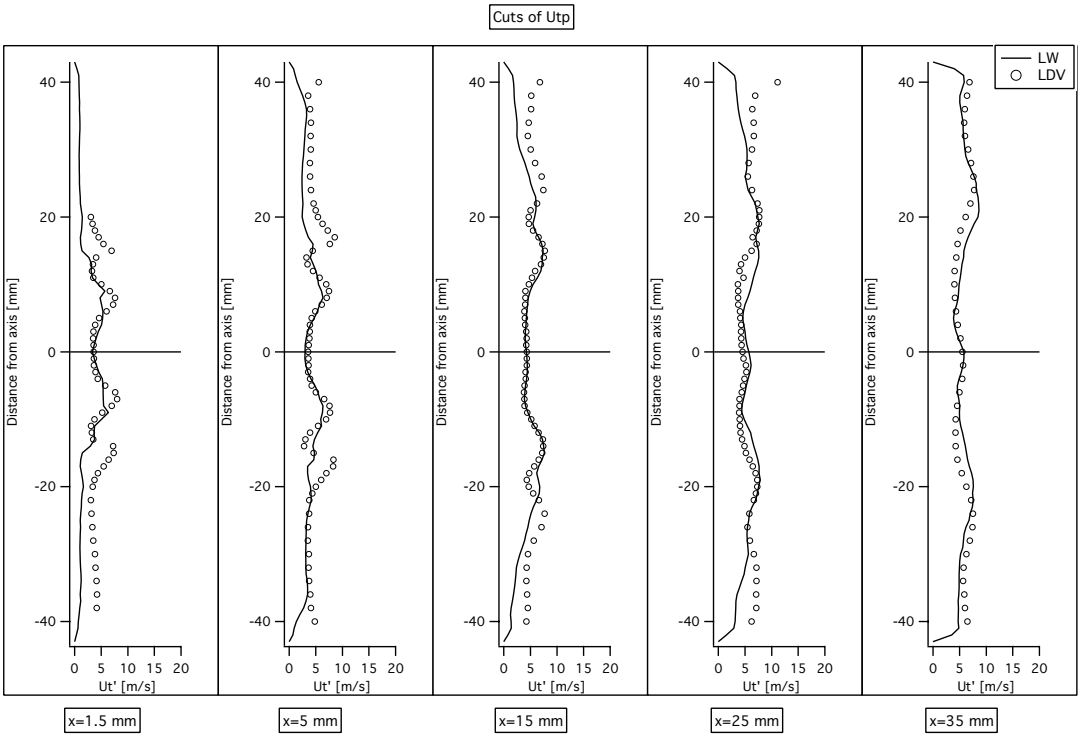

Figure 5.14: RMS tangential velocity in central plane for configuration 2. ○ LDV; ——LES.

Chapter 6

Conclusions

The future tools for gas turbine designs will be based on classical Reynolds Averaged codes to predict mean flows but will also rely on Large Eddy Simulation tools coupled to acoustic codes. This paper has presented the basis of LES adapted to gas turbine flows, the development of acoustic codes and the application to two typical gas turbine burners installed in laboratory combustion chambers. The analysis of the LES reveals that a strong precessing vortex core (PVC) is observed for non reacting flows in both cases . This vortex disappears when combustion is activated. Unsteady pressure fields are also very different for cold and reacting flow: maximum pressure oscillations are observed in the PVC zone for the cold flow; with combustion, the pressure oscillations maxima are located at the chamber walls and have an acoustic structure corresponding to a coupled transverse-longitudinal mode in the first configuration. This structure is confirmed by using a three-dimensional Helmholtz code. In the second configuration, a low-frequency quarter-wave mode is found and its structure is confirmed using a one-dimensional acoustic code.

Acknowledgments

Certain numerical simulations have been conducted on the computers of CINES and IDRIS french national computing centers. Simulations have been supported partly by Siemens and by the EC program (FP5) PRECCINSTA.

Chapter 7

References

- Angelberger, C., Egolfopoulos, F. & Veynante, D. 2000 Large Eddy Simulations of chemical and acoustic effects on combustion instabilities. *Flow Turb. and Combustion* **65,** 205-22.
- Angelberger, D., Veynante, D., Egolfopoulos, F. & Poinsot, T. 1998 Large Eddy Simulations of combustion instabilities in premixed flames. *Summer Program,* Center for Turbulence Research, NASA Ames/Stanford Univ., 61-82.
- Baum, M., Poinsot, T. J. & Thévenin, D. 1994 Accurate boundary conditions for multicomponent reactive flows. *J. Comput. Phys.* **116,** 247-261.
- Butler, T. D. & O'Rourke, P. J. 1977 A numerical method for two-dimensional unsteady reacting flows. *16th Symp. (Int.) on Combustion,* The Combustion Institute, 1503 - 1515.
- Candel, S., Huynh, C. & Poinsot, T. 1996 Some modeling methods of combustion instabilities. In *Unsteady combustion,* pp. 83-112, Nato ASI Series, Kluwer Academic Publishers, Dordrecht.
- Caraeni, D., Bergström, C. & Fuchs, L. 2000 Modeling of Liquid Fuel Injection, Evaporation and Mixing in a Gas Turbine Burner Using Large Eddy Simulation. *Flow Turb. and Combustion* **65,** 223-244.
- Chakravarthy, V. K. & Menon, S. 2000 Subgrid Modeling of Turbulent Premixed Flames in the Flamelet Regime. *Flow Turb. and Combustion* **65,** 133-161.
- Charlette, F., Veynante, D. & Meneveau, C. 2002 A power-law wrinkling model for LES of premixed turbulent combustion: Part I - non-dynamic formulation and initial tests. *Combust. Flame* **131,** 159-180.
- Colin, O., Ducros, F., Veynante, D. & Poinsot, T. 2000 A thickened flame model for large eddy simulations of turbulent premixed combustion. *Phys. Fluids* **12,** 1843-1863.
- Colin, O. & Rudgyard, M. 2000 Development of high-order Taylor-Galerkin schemes for unsteady calculations. *J. Comput. Phys.* **162,** 338-371.
- Crighton, D. G., Dowling, A., Ffowcs Williams, J., Heckl, M. & Leppington, F. 1992 *Modern methods in analytical acoustics.* Springer Verlag.

- Crocco, L. 1969 Research on combustion instability in liquid propellant rockets. *12th Symp. (Int.) on Combustion,* The Combustion Institute, Pittsburgh, 85-99.
- Dellenback, P., Metzger, D. & Neitzel, G. 1988 Measurement in turbulent swirling flows through an abrupt axisymmetric expansion. *AIAA Journal* **13,** 669-681.
- Desjardins, P. E. & Frankel, S. H. 1999 Two dimensional Large Eddy Simulation of soot formation in the near field of a strongly radiating nonpremixed acetylene-air jet flame. *Combust. Flame* **119,** 121-133.
- Duchamp de Lageneste, L. & Pitsch, H. 2001 Progress in large eddy simulation of premixed and partially premixed turbulent combustion. In *Annual research briefs,* pp. 61-82, Center for Turbulence Research, Stanford Univ./NASA-Ames.
- Ducros, F., Comte, P. & Lesieur, M. 1996 Large-eddy simulation of transition to turbulence in a boundary layer developing spatially over a flat plate. *J. Fluid Mech.* **326,** 1-36.
- Forkel, H. & Janicka, J. 2000 Large-Eddy Simulation of a Turbulent Hydrogen Diffusion Flame. *Flow Turb. and Combustion* **65,** 163-175.
- Fureby, C. & Möller, S. I. 1995 Large eddy simulations of reacting flows applied to bluff body stabilized flames. *AIAA Journal* **33,** 2339.
- Gamet, L., Ducros, F., Nicoud, F. & Poinsot, T. 1999 Compact Finite Difference Schemes on Non-Uniform Meshes. Application to Direct Numerical Simulations of Compressible Flows. *International Journal for Numerical Methods in Fluids* **29,** 159-191.
- Guo, B., Langrish, T. & Fletscher, D. 2001 Simulationof turbulent swirl flow in an axisymmetric sudden expansion. *AIAA Journal* **39,** 96-102.
- Gupta, A. K., Lilley, D. G. & Syred, N. 1984 *Swirl flows*. Abacus Press.
- Hsiao, G., Pandalai, R., Hura, H. & Mongia, H. 1998 Combustion dynamic modelling for gas turbine engines. AIAA Paper 98-3380,
- Jones, W. P. & Lindstedt, R. P. 1988 Global Reaction Schemes for Hydrocarbon Combustion. *Combust. Flame* **73,** 222-233.
- Kaufmann, A., Nicoud, F. & Poinsot, T. 2002 Flow forcing techniques for numerical simulation of combustion instabilities. *Combust. Flame* **131,** 371-385.
- Keller, J. O., Vaneveld, L., Korschelt, D., Hubbard, G. L., Ghoniem, A. F., Daily, J. W. & Oppenheim, A. K. 1981 Mechanism of instabilities in turbulent combustion leading to flashback. *AIAA Journal* **20,** 254-262.
- Kempf, A., Forkel, H., Chen, J.-Y., Sadiki, A. & Janicka, J. 2000 Large-eddy simulation of a counterflow configuration with and without combustion. *Proc. of the Combustion Institute* **28,** 35-40.
- Kinsler, L. E., Frey, A. R., Coppens, A. B. & Sanders, J. V. 1982 *Fundamental of acoustics*. John Wiley.

- Krueger, U., Hueren, J., Hoffmann, S., Krebs, W., Flohr, P. & Bohn, D. 2000 Prediction and measurements of thermoacoustic improvements in gas turbines with annular combustion systems. *ASME TURBO EXPO 2000,* ASME Paper 2000-GT-0095,

- Lartigue, G., Moureau, V., Sommerer, Y., Angelberger, C., Colin, O. & Poinsot, T. 2003 High-order methods for DNS and LES of compressible multi-component reacting flows on fixed and moving grids. *J. Comput. Phys.* submitted.

- Lele, S. 1992 Compact finite difference schemes with spectral like resolution. *J. Comput. Phys.* **103,** 16-42.

- Lucca-Negro, O. & O'Doherty, T. 2001 Vortex breakdown: a review. *Prog. Energy Comb. Sci.* **27,** 431-481.

- Légier, J.-P., Poinsot, T. & Veynante, D. 2000 Dynamically thickened flame Large Eddy Simulation model for premixed and non-premixed turbulent combustion. *Summer Program 2000,* 157-168.

- Nicoud, F. & Ducros, F. 1999 Subgrid-scale stress modelling based on the square of the velocity gradient. *Flow Turb. and Combustion* **62,** 183-200.

- Paschereit, C. O., Flohr, P. & Schuermans, B. 2001 Prediction of combustion oscillations in gas turbine combustors. *39th AIAA Aerospace Sciences Meeting and Exhibit,* AIAA Paper 2001-0484,

- Peters, N. 2000 *Turbulent combustion.* Cambridge University Press.

- Pierce, C. D. & Moin, P. 1998 Large eddy simulation of a confined coaxial jet with swirl and heat release. *29th Fluid Dynamics Conference,* AIAA Paper 98-2892,

- Pitsch, H. & Duchamp de la Geneste, L. 2002 Large Eddy Simulation of Premixed Turbulent Combustion using a level-set approach. *Proc of the Comb. Institute* **29,** 2001-2008.

- Pitsch, H. & Steiner, H. 2000 Large Eddy Simulation of a Turbulent Piloted Methane/Air Diffusion Flame (Sandia Flame D). *Phys. Fluids* **12,** 2541-2554.

- Poinsot, T. & Lele, S. 1992 Boundary conditions for direct simulations of compressible viscous flows. *J. Comput. Phys.* **101,** 104-129.

- Poinsot, T., Trouvé, A., Veynante, D., Candel, S. & Esposito, E. 1987 Vortex driven acoustically coupled combustion instabilities. *J. Fluid Mech.* **177,** 265-292.

- Poinsot, T. & Veynante, D. 2001 *Theoretical and numerical combustion.* R.T. Edwards.

- Poinsot, T., Veynante, D., Bourienne, F., Candel, S., Esposito, E. & Surjet, J. 1988 Initiation and suppression of combustion instabilities by active control. *22nd Symp. (Int.) on Combustion,* The Combustion Institute, Pittsburgh, 1363-1370.

- Polifke, W., Poncet, A., Paschereit, C. O. & Doebbeling, K. 2001 Control of Thermoacoustic Instabilities in a Premixed Combustor by Fuel Modulation. *J. Sound Vibration* **245,** 483-510.

- Rayleigh, L. 1878 The explanation of certain acoustic phenomena. *Nature* **July 18,** 319-321.
- Rogers, D. E. & Marble, F. E. 1956 A mechanism for high frequency oscillations in ramjet combustors and afterburners. *Jet Propulsion* **26,** 456-462.
- Sagaut, P. 2000 *Large Eddy Simulation for incompressible flows*. Springer-Verlag.
- Scotti, A., Meneveau, C. & Fatica, M. 1997 Generelized Smagorinski model for anisotropic grids. *Phys. Fluids* **9,** 1856-1858.
- Scotti, A., Meneveau, C. & Lilly, D. K. 1993 Generelized Smagorinski model for anisotropic grids. *Phys. Fluids* **5,** 2306-2308.
- Selle, L., Lartigue, G., Poinsot, T., Kaufman, P., Krebs, W. & Veynante, D. 2002 Large Eddy Simulation of turbulent combustion for gas turbines with reduced chemistry. In *Proc. of the Summer Program,* pp. 333-345, Center for Turbulence Research, NASA Ames/Stanford Univ.
- Vasilyev, O. V., Lund, T. S. & Moin, P. 1998 A general class of commutative filters for LES in complex geometries. *J. Comput. Phys.* **146,** 82-104.
- Weller, H. G., Tabor, G., Gosman, A. D. & Fureby, C. 1998 Application of a flame-wrinkling LES combustion model to a a turbulent mixing layer. *27th Symp. (Int.) on Combustion,* The Combustion Institute, Pittsburgh, 899 - 907.
- Williams, F. A. 1985 *Combustion theory.* Benjamin Cummings.
- Yang, V. & Culick, F. E. C. 1986 Analysis of low-frequency combustion instabilities in a laboratory ramjet combustor. *Combust. Sci. Tech.* **45,** 1-25.